
White Rose Research Online

eprints@whiterose.ac.uk
https://eprints.whiterose.ac.uk
Universities of Leeds, Sheffield and York

Deposited via The University of Leeds.

White Rose Research Online URL for this paper:
https://eprints.whiterose.ac.uk/id/eprint/246950/

Version: Accepted Version

**Article:**
Lei, X., Yang, Y., Fang, K. et al. (2026) Multi-scale characterization and statistical analysis on aging behaviors of SBS modified asphalt exposed to plateau environments: Morphology, rheology and mechanism. Construction and Building Materials, 546. 148512. ISSN: 0950-0618

https://doi.org/10.1016/j.conbuildmat.2026.148512

This is an author produced version of an article published in Construction and Building Materials, made available via the University of Leeds Research Outputs Policy under the terms of the Creative Commons Attribution License (CC-BY), which permits unrestricted use, distribution and reproduction in any medium, provided the original work is properly cited.

**Reuse**
This article is distributed under the terms of the Creative Commons Attribution (CC BY) licence. This licence allows you to distribute, remix, tweak, and build upon the work, even commercially, as long as you credit the authors for the original work. More information and the full terms of the licence here: https://creativecommons.org/licenses/

**Takedown**
If you consider content in White Rose Research Online to be in breach of UK law, please notify us by emailing eprints@whiterose.ac.uk including the URL of the record and the reason for the withdrawal request.





# Multi-Scale Characterization and Statistical Analysis on Aging Behaviors of SBS Modified Asphalt Exposed to Plateau Environments: Morphology, Rheology and Mechanism

Xiaoqiu LEI[a,b], Yiwang YANG[c], Kun FANG[c], Guangwei CHEN[a,b], Ali RAHMAN[b*], Dongya REN[a,b,c**]

a. SWJTU-LEEDS Joint School, Southwest Jiaotong University, Chengdu, Sichuan, 610031, China

b. Faculty of Engineering and Physical Sciences, University of Leeds, Leeds, LS2 9JT, United Kingdom

c. School of Civil Engineering, Southwest Jiaotong University, Chengdu, Sichuan, 610031, China

*Corresponding author: Dongya REN, E-mail: dongyaren@swjtu.edu.cn, Ali RAHMAN, E-mail: A.Rahman1@leeds.ac.uk

---

**Abstract:** The extreme climatic conditions on the Qinghai-Tibet Plateau (QTP), characterized by intense ultraviolet (UV) radiation and drastic temperature fluctuations, exert severe aging threats to styrene-butadiene-styrene modified asphalt (SBSMA). To investigate the aging behavior and performance evolution of SBSMA in this complex environment, this study developed a coupled plateau aging (CPA) protocol based on field meteorological parameters, with individual UV aging (UVA) serving as the control. On this basis, the multi-scale morphological characteristics of the aged SBSMA were characterized via surface observation, fluorescence microscopy (FM), and atomic force microscopy (AFM). The rheological properties of the SBSMA at a wide temperature range were evaluated through temperature sweep (TS), multiple stress creep recovery (MSCR), linear amplitude sweep (LAS), and bending beam rheometer (BBR) tests. The evolution in the chemical compositions of the aged binder were analyzed using Fourier transform infrared spectroscopy (FT-IR), gel permeation chromatography (GPC), and thin-layer chromatography with flame ionization detection (TLC-FID). Furthermore, Hierarchical cluster analysis (HCA) and Spearman rank correlation analysis (SRCA) were integrated to reveal the correlations between microscopic mechanism

indicators and macroscopic rheological parameters, thereby clarifying the influence patterns of aging mechanisms on various rheological performances. The results indicated that: (1) Under long-term CPA, severe cracks developed on the surface of the aged SBSMA, accompanied by a significant reduction in the fluorescent area and a substantial increase in micro roughness. (2) The overall performance of the SBSMA continuously degraded during the aging duration, and the deterioration effects under CPA were more pronounced than those under UVA. (3) Under both aging conditions, the SBSMA aging process followed a two-stage mechanism, shifting from being dominated by SBS degradation to being dominated by asphalt oxidation, with the transition occurring earlier under CPA. (4) When exposed to long-term aging, CPA resulted in a lower oxidation degree of the matrix asphalt, while inducing earlier and more thorough SBS degradation. (5) The microscopic mechanism indicators could be categorized into SBS degradation cluster and asphalt oxidation cluster. $I_{PB}$ and $I_{SBS}$ were categorized into the SBS degradation cluster, whereas $I_{C=O}$, $I_{S=O}$, *PDI*, and $I_C$ belonged to the asphalt oxidation cluster; the classification of $R_a$ and $R_q$ varied depending on the aging conditions. These findings provide a basis for investigating the deterioration of SBSMA in plateau regions.

**Keywords:** SBS modified asphalt; Qinghai-Tibet Plateau; Aging behaviors; Multi-scale characterization; Hierarchical cluster analysis; Spearman rank correlation analysis

# 1 Introduction

Lying in western China, covering about 2.5 million km$^2$, and with a mean elevation of 4500 m, the Qinghai-Tibet Plateau (QTP) is one of the largest plateaus in the world [1–3]. The region is sparsely populated, with roughly 9.67 million residents and an average density below 10 persons per km$^2$. As the key channel connecting areas and sustaining the movement of supplies, highways are of considerable social significance for the region, and their durability therefore has direct practical impacts.

Asphalt pavement constitutes the predominant surface form for highways in the QTP region, yet the harsh and complex local climate poses heavy demands on pavement service performance. Specifically, the QTP receives the highest solar radiation intensity in China, which results in severe ultraviolet aging of the asphalt surface layer. The region also experiences wide diurnal temperature swings and rapid temperature changes, with the daily temperature difference reaching 40 °C in certain

areas, rendering pavements prone to cracking under thermal stress[4–6]. Under the combined effect of ultraviolet radiation and temperature fluctuation, pavement performance degrades rapidly and the service life is sharply curtailed. A field survey of a 440 km stretch of the Qinghai-Tibet Highway (QTH) reported cracking, raveling, and similar distress on more than 85% of the pavement, with over two-thirds of the sections failing to meet the required pavement quality index (PQI), reflecting the poor service status of asphalt pavements across the QTP region[7].

Aging of asphalt binder is one of the most critical factors restricting pavement performance in QTP area. Aging refers to the transformation process of components and properties of binder under the external effects of sunlight, temperature and oxygen [8–10]. Asphalt aging involves complex physical and chemical processes, more than 15 mechanisms have been proposed to explain this behavior, among which the volatilization, oxidation and spatial hardening are the three main mechanisms widely accepted [11]. The above aging mechanism is mainly triggered in two stages, one is the thermal aging of binder caused by heating in the construction stage, and the other is the ultraviolet (UV) aging caused by long-term solar radiation during the service period. As a consequence, aged binder becomes brittle and rigid, the deformation relaxation capacity decreases, and the adhesion to the aggregate interface also reduces[12,13]. Although the aging of binders is unavoidable in nature, the harsh environment of the QTP significantly accelerates this process, leading to premature deterioration of pavement performance and becoming the main cause of its diseases in this region.

SBS modified asphalt (SBSMA) exhibits superior performance at a wide temperature range, making it an ideal material for pavement in QTP area. Owing to the presence of the polymer phase, however, the aging behavior of SBSMA is different from that of conventional virgin binder[1,14]. Liu et al. investigated the natural aging behavior of virgin asphalt and SBSMA in cold regions, noting that virgin asphalt mainly undergoes oxidation, whereas SBSMA undergoes simultaneous degradation of SBS and oxidation of asphalt[15]. Liang et al. pointed out that due to polymer degradation, the long-term aging resistance of SBSMA is weaker than that of base asphalt[16]. Ju et al. found that UV aging of SBSMA is dominated by polymer fracture, and the degraded SBS further reduces the uniformity of binder[17]. Besides, SBSMA aging is highly environment-dependent, exhibiting diverse aging behaviors across varying environments. For instance, Zhang et al. reported

that the coupling of UV radiation and low temperatures in plateau areas drastically impairs the relaxation capability of SBSMA, resulting in a much higher level of deterioration than exposure to low temperatures alone[2]. In an investigation of SBSMA aging under intense UV radiation and freeze-thaw cycles in northwest China, He et al. found that UV radiation exerts a pronounced impact on asphalt binder aging, whereas freeze-thaw cycles dominate the degradation of asphalt mixtures[18]. Through multi-regional field aging tests, Ma et al. observed that the aging of SBSMA in cold, high-altitude areas is dominated by surface aging induced by UV radiation, whereas it exhibits deeper aging characteristics in warm, low-altitude areas due to stronger thermal-oxidative diffusion[19]. Notably, the coupling of UV radiation with other environmental factors does not invariably accelerate asphalt aging. For instance, Zhao et al. noted that water can mitigate the UV aging of asphalt to some extent, as evidenced by the finding that single UV aging inflicted even more severe microstructural damage on SBSMA than light-heat-water coupled aging[20]. These findings indicate that the aging behavior of SBSMA is governed by the synergistic effects of multiple environmental stressors, rather than a simple linear summation of individual factors. Given the unique climatic conditions of the QTP, the aging behavior of SBSMA is bound to differ from that of virgin asphalt or SBSMA serving in other regions. Consequently, there is an urgent need to elucidate the aging and degradation behaviors under actual QTP service conditions.

Unlike thermal aging, for which standardized laboratory methods are available, no unified protocol has been established for UV aging. Existing studies generally use customized UV, high pressure mercury, or xenon lamps, resulting in considerable variations in wavelength, irradiance, temperature, duration, and film thickness[11,21,22]. Hu et al.[23] compared different UV wavebands and film thicknesses but focused mainly on the effects of individual parameters rather than environmental coupling. Wang et al.[24] determined laboratory exposure from the UV radiation dose of the QTP and aged binders at a constant temperature of 45°C, without considering the large diurnal temperature fluctuations of the region. Xie et al.[25] simulated high-altitude UV exposure at 35°C and evaluated the low-temperature performance of the aged binders, while UV radiation and low temperature were considered separately. These studies provide valuable insights into asphalt aging behavior, but their findings are based on specific experimental conditions and have limited applicability to the QTP. Moreover, advances in characterization techniques provide a technical basis

for understanding material behavior across various scales. Published studies have applied multiscale approaches to investigate the aging behavior of both base and modified asphalt binders[26–28], demonstrating their value in revealing the mechanisms governing binder deterioration. Given the complex aging behavior of SBSMA under the environmental stresses of the QTP, combining a targeted aging protocol with multiscale characterization is essential for improving the environmental relevance of laboratory aging simulation and elucidating the underlying aging mechanisms.

In summary, this study investigates the aging behavior and mechanism of SBSMA subject to the plateau environment. To achieve this, a laboratory-accelerated aging protocol was first developed utilizing field-measured meteorological data. On this basis, the multi-scale morphological evolution of the aged SBSMA was comprehensively characterized from macroscopic to microscopic levels; meanwhile, its rheological performance was evaluated over a broad temperature range, and the underlying mechanisms governing chemical composition variations were elucidated. Ultimately, Hierarchical cluster analysis (HCA) and Spearman rank correlation analysis (SRCA) were combined to validate the aging mechanisms. This study provides useful insights into the aging behavior of SBSMA in plateau regions.

The flowchart of this study is shown in Fig.1.

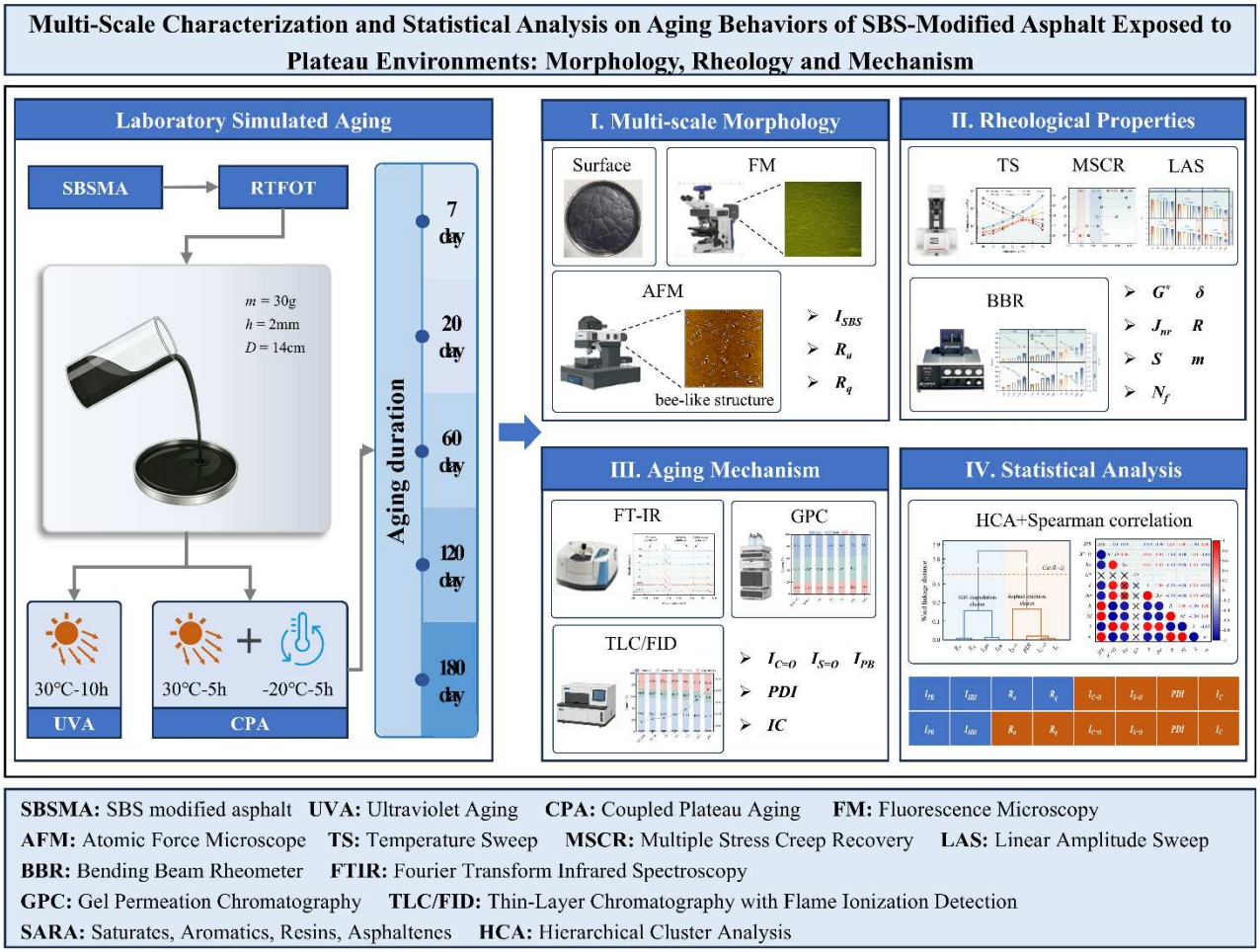



**Fig 1. Research flowchart of this study**

# 2 Materials and methods

## 2.1 Service environment of the QTP region

The QTP has a harsh, cold continental climate characterized by intense solar radiation and drastic temperature variations. It is among the regions with the strongest UV radiation worldwide, while the maximum temperature difference can even approach 50°C. These severe environmental conditions make pavements in this region highly susceptible to distress. Fig.2 presents the direct normal irradiance (DNI) data for the QTP, temperature conditions at representative locations, and typical pavement distresses along the QTH.

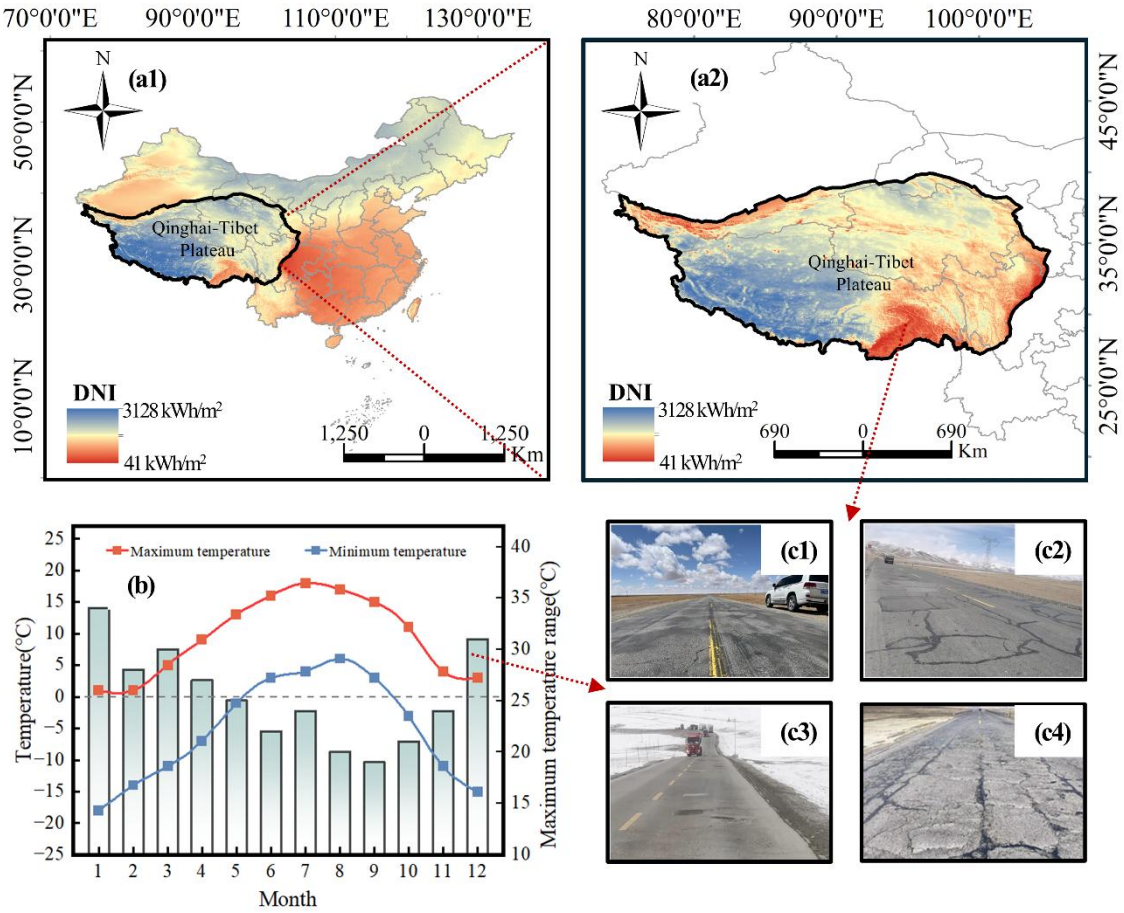



**Fig 2. Highway service environment in the QTP region: (a)spatial distribution of DNI; (b)representative ambient temperatures; (c)typical pavement distresses along the QTH**

## 2.2 Laboratory accelerated aging

### 2.2.1 Asphalt binder

The binder used in this study was a Class I-A SBS modified asphalt obtained from Gansu Road & Bridge Shanjian Group (Lanzhou, China). Its specific technical indicators are listed in Tab.1.

**Tab 1. Technical parameters of SBSMA**

| Items | Results | Technical indexes | Standard |
|---|---|---|---|
| Penetration(25°C,100 g,5s)/0.1 mm | 122 | 110~130 | T0604 |
| Penetration Index (PI) | 0.2 | ≥-1.2 | |
| Softening point/°C | 82 | ≥50 | T0606 |
| 5°C ductility/cm | 102 | 100 | T0605 |
| Flash point/°C | 260 | ≥230 | T0611 |
| Solubility/% | 99.8 | ≥99.0 | T0607 |

| RTFOT | | | |
|---|---|---|---|
| Mass loss/% | -0.12 | ±1.0 | T0610 |
| Residual penetration ratio（25℃）/% | 72 | ≥55 | T0604 |
| 5℃ Residual ductility/cm | 75 | ≥70 | T0605 |

### 2.2.2 Sample preparation

Asphalt binder aging is a continuous process, comprising short-term aging during construction and long-term UV aging throughout the pavement service life. To replicate this succession, the virgin asphalt was initially subjected to thermo-oxidative aging, followed by a subsequent coupled UV radiation and large temperature fluctuation aging protocol. The initial thermo-oxidative conditioning was performed via the Rolling Thin-Film Oven Test (RTFOT) in compliance with ASTM D2872-22. Briefly, 35 g of asphalt was weighed into each RTFOT bottle and conditioned at 163 °C for 85 min with a rotation speed of 15 r/min. Afterward, the short-term aged asphalt was transferred into customized aging pans for subsequent environmental conditioning.

To date, a consensus on the penetration threshold of UV radiation within asphalt films remains elusive, with literature reporting film thicknesses spanning from 10 μm to 3 mm[29]. An excessively thick film induces a non-uniform aging gradient that misrepresents field conditions, whereas an ultra-thin film introduces severe fabrication difficulties. Balancing these limitations, an asphalt film thickness of 2 mm was adopted herein. To achieve this, 30 g of molten asphalt was uniformly cast into a 14 cm diameter sample pan before being exposed within the environmental chamber.

### 2.2.3 Equivalent conversion of aging time

Laboratory accelerated aging was conducted using a customized environmental chamber equipped with six UVA-340 fluorescent lamps, a specimen platform, and a temperature control unit. The UVA-340 lamps were selected because their spectral distribution closely mimics that of natural sunlight in the 295–360 nm wavelength range, ensuring an accurate simulation of short-wave solar UV radiation[30]. These lamps, each with a 40 W UV radiation capacity, were arranged in parallel at 8 cm intervals and positioned approximately 10 cm above the specimen platform.

The relationship between laboratory and field UV aging was established based on the principle

of equal average daily total UV radiation. For simplicity of calculation, the average annual solar radiation in this study was taken as 800 kJ/cm², wherein the UV component constituted approximately 5%[31]. With the asphalt samples centered directly underneath the lamp array, the effective irradiance striking the specimen surface represents a superposition of the intensities from the light sources. It was determined that 1.5 hour of indoor accelerated aging effectively replicates 1 day of natural outdoor UV exposure for the asphalt binder.

### 2.2.4 Coupled aging process

Owing to the heat accumulation effect inherent to black asphalt pavements, the pavement surface temperature generally exceeds the ambient air temperature by approximately 25 °C[30]. Considering the wider temperature variations experienced by pavement surfaces, chamber temperatures of 30 °C and −20 °C were selected as the worst conditions to amplify the influence of temperature variations in the QTP. Each cycle consisted of 5 h of high-temperature UV exposure and 5 h of low-temperature UV exposure, thereby yielding a cyclic temperature differential of 50 °C. The 5 h duration provided sufficient conditioning at each target temperature while ensuring that each aging interval contained an integral number of complete cycles. To differentiate the distinct mechanisms induced by the coupled plateau environment on SBSMA, conventional asphalt samples conditioned under sole UV radiation at a constant temperature of 30 °C served as the control group.

Five aging intervals of 7, 20, 60, 120, and 180 days were selected, focusing primarily on the first half year following pavement construction. The specimens subjected to coupled UV and temperature aging were designated as CPA-X (Coupled Plateau Aging), whereas those subjected to UV aging alone were named as UVA-X (Ultraviolet Aging), where X represents the aging duration in days.

The detailed scheme of the aging test is illustrated in Fig.3, and the designations of all experimental groups are compiled in Tab.2.

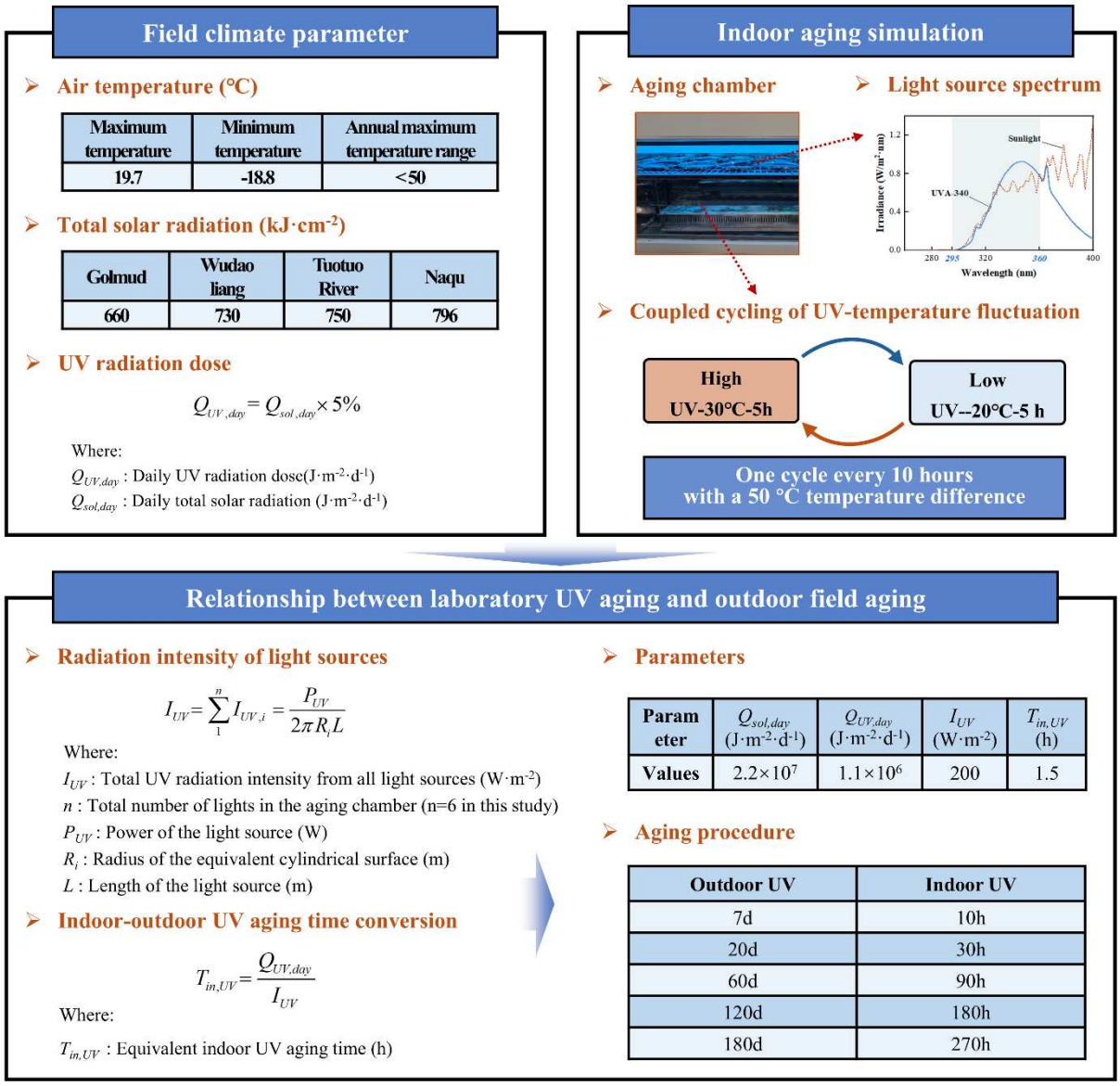



**Fig 3. Indoor simulation procedure of CPA**

**Tab 2. Summary of test groups**

| Binder | Aging Procedure | Code |
|---|---|---|
| SBSMA | Unaged | SBS-OG |
| | RTFOT | SBS-R |
| | RTFOT+CPA/UVA-7D | CPA/UVA-7D |
| | RTFOT+CPA/UVA-20D | CPA/UVA-20D |
| | RTFOT+CPA/UVA-60D | CPA/UVA-60D |
| | RTFOT+CPA/UVA-120D | CPA/UVA-120D |
| | RTFOT+CPA/UVA-180D | CPA/UVA-180D |

## 2.3 Morphology characterization

### 2.3.1 Surface macroscopic morphology

When subjected to temperature fluctuations and UV radiation, the morphology of asphalt binders undergoes alterations induced by various physical and chemical processes. Since the sample surface is directly exposed to the external aging environment, it exhibits the most pronounced aging phenomena. Consequently, visual inspection was performed to examine the surface states of the samples across diverse aging regimes and intervals, aiming to qualitatively characterize the morphological features during environmental conditioning.

To further characterize the morphology of cracks, field emission scanning electron microscopy (JEOL JSM-7800F, Japan) was utilized to examine the cracks on sample's surfaces. The accelerating voltage was set to 15 kV, and images were acquired at magnifications of 100×, 400×, and 1000×.

### 2.3.2 SBS distribution morphology

The aging of SBSMA is generally accompanied by the degradation of SBS polymers, which is the intrinsic reason why the aging behavior of SBSMA differs from that of neat asphalt. Since SBS contains excitable fluorescent functional groups under ultraviolet light, the bright domains represent the SBS-rich phase, while the dark domains represent the asphalt-rich phase under a fluorescence microscope (FM). Consequently, FM is suitable to characterize the mesoscopic distribution of SBS within aged binders[32].

A fluorescence microscope (Viyee V5800, China) was employed to observe the SBSMA specimens at 10× magnification and 25°C, with five fields of view examined for each sample. All images were acquired under identical settings. Before segmentation, each image was converted to grayscale, uneven illumination was corrected, and isolated noise was suppressed using a median filter. The corrected grayscale values were then linearly normalized using the same fixed intensity range for all images. Following the modified Otsu method proposed by Singh et al.[33], Otsu's between-class variance and Kapur's entropy were combined to dynamically determine the optimal threshold for each image. Using Python scripts, the average area fraction of the fluorescent phase was extracted, and the SBS content index, $I_{SBS}$, was calculated according to Eq.(1).

$$I_{SBS} = \frac{A_{SBS}}{A_{SBSMA}} \times 100\% \quad (1)$$

Where $A_{SBS}$ and $A_{SBSMA}$ represent the area occupied by the SBS phase and the gross area of the field of view, respectively.

### 2.3.3 Surface microscopic morphology

The macroscopic changes in asphalt surface morphology originate from alterations in its microstructure; thus, observations at the microscopic scale facilitate a deeper explanation of the aging behaviors of SBSMA. Atomic force microscopy (AFM) is a nanoscale imaging technique capable of characterizing the phase distribution on asphalt surfaces[34]. In this study, an AFM instrument (Oxford Cypher S, USA) was employed, operating in tapping mode, to scan a 20 × 20 μm² area of the SBSMA specimens at a temperature of 25°C. To prepare the samples, small pieces of the upper aged film were collected with tweezers, placed on 20mm × 20mm glass coverslips, and then conditioned in an oven at 165°C for approximately 1 min to allow natural self-leveling.

The surface roughness of asphalt is intimately correlated with its microscopic phase distribution. Average roughness ($R_a$) and root-mean-square roughness ($R_q$) were adopted to quantitatively evaluate the surface roughness of the asphalt binders, with higher $R_a$ and $R_q$ values indicating a rougher asphalt surface[35]. Five regions were tested per specimen, and the results were calculated according to Eqs. (2) and (3) and averaged.

$$R_a = \frac{\iint |h(x,y) - h_0| ds}{\iint ds} \quad (2)$$

$$R_q = \sqrt{\frac{\iint [h(x,y) - h_0]^2 ds}{\iint ds}} \quad (3)$$

Where $h(x, y)$ represents the local height at coordinates, $s$ is the scanning area, and $h_0$ is the reference baseline height.

## 2.4 Rheological properties

The rheological behavior of asphalt binders, which represents the comprehensive mechanical response involving both elastic and viscous deformations, is a macroscopic manifestation of their internal microstructure and molecular characteristics, and is intimately correlated with the field road

performance. In this study, the rheological properties of the aged SBSMA were evaluated over a broad temperature range using a Dynamic Shear Rheometer (TA Instruments, USA) and a Bending Beam Rheometer (CANNON, USA) to investigate the impact of the two aging modes. Each measurement was conducted in quintuplicate, with the average values adopted.

### 2.4.1 Viscoelastic behavior

The temperature sweep test was conducted in accordance with AASHTO T 315-06. The test configuration utilized a plate diameter of 25 mm and a gap of 1 mm. The temperature range was set from 40 °C to 76 °C with an interval of 6 °C, at a constant angular frequency of 10 rad/s and a heating rate of 2 °C/min. The complex shear modulus ($G^*$) and phase angle ($\delta$) were obtained to evaluate the deformation resistance of aged SBSMA.

To quantitatively evaluate the aging susceptibility of the binders, the Aging Index ($AI$) was adopted[11]. The $AI$ for $G^*$ and $\delta$ was calculated as follows:

$$AI_{\mathrm{p}} = \frac{P_{\mathrm{Aged}} - P_{\mathrm{OG}}}{P_{\mathrm{OG}}} \times 100\% \tag{4}$$

Where, $P_{\mathrm{Aged}}$ and $P_{\mathrm{OG}}$ denote the values of the performance indices ($G^*$, $\delta$) for the aged and unaged specimens, respectively.

### 2.4.2 Permanent deformation resistance

The temperature sweep test neglects the elastic recovery capacity of the polymer network in modified asphalt, which may lead to an underestimation of the deformation resistance of SBSMA[36]. The multiple stress creep recovery (MSCR) test can capture the delayed elastic response of SBSMA and serves as a supplementary test to evaluate its rheological properties at high temperature.

The MSCR test was conducted in accordance with the ASTM D7405 standard. The test employed a stress-controlled mode, consisting of 20 loading cycles at a creep stress of 0.1 kPa, followed by 10 loading cycles at 3.2 kPa. Each cycle lasted 10 s, comprising a 1 s loading period and a 9 s unloading recovery period. Based on the performance grade (PG) of the SBSMA, the test temperature was set at 70 °C. The strain recovery ratio $R$ was used to quantify the elastic recovery performance, with a higher $R$ indicating better elasticity; the non-recoverable creep compliance $J_{\mathrm{nr}}$

was used to evaluate the resistance to permanent deformation, with a higher $J_{nr}$ indicating poorer deformation resistance[37]. The calculation formulas for these two parameters are as follows:

$$R = \frac{(\varepsilon_c - \varepsilon_r)}{\varepsilon_c - \varepsilon_0} \times 100\% \quad (5)$$

$$J_{nr} = \frac{(\varepsilon_r - \varepsilon_0)}{\delta} \quad (6)$$

Where $\varepsilon_0$, $\varepsilon_c$ and $\varepsilon_r$ represent the initial strain, the strain at the end of the creep phase, and the residual strain after the recovery phase, respectively; $\delta$ denotes the applied stress level; and $R$ and $J_{nr}$ are each taken as the average value over 10 cycles.

### 2.4.3 Fatigue resistance

The linear amplitude sweep (LAS) test was conducted in accordance with AASHTO TP 101-12 to evaluate the fatigue resistance of asphalt binders at intermediate temperatures. An 8 mm parallel plate geometry with a 2 mm gap was used at 25°C. The test consisted of two stages. First, a frequency sweep was performed at a constant strain of 0.1% over the frequency range of 0.1–30 Hz to determine the rheological parameter α. Subsequently, an amplitude sweep was conducted at 10 Hz, during which the sinusoidal shear strain amplitude increased linearly from 0.1% to 30%[36,38]. Fatigue life was calculated using the viscoelastic continuum damage (VECD) framework, with $G^*\sin\delta$ adopted as the material integrity parameter. Fatigue failure was defined as the damage state corresponding to a 35% reduction in the undamaged $G^*\sin\delta$[39,40]. Given the importance of fatigue life at high strain levels for practical pavement performance, the fatigue lives of aged SBSMA specimens were calculated at strain levels of 5%, 10%, and 15% using the following equation:

$$N_f = A_{35}\left(\gamma_{max}\right)^{(-B)} \quad (7)$$

Where $N_f$ is the predicted fatigue life, $\gamma_{max}$ is the applied strain level, $A_{35}$ is the model coefficient determined from the 35% reduction criterion of $G^*\sin\delta$, and B is the strain sensitivity exponent. The fatigue lives of the aged SBSMA specimens were calculated at strain levels of 5%, 10%, and 15%.

### 2.4.4 Cracking resistance

According to ASTM D6648, the rheological properties of the aged SBSMA at low temperature were evaluated using the bending beam rheometer (BBR) test. During the test, the asphalt specimen

was subjected to a constant load at the specified temperature. After 60 seconds of loading, the creep stiffness (*S*-value) and creep rate (*m*-value) were determined from the load-deflection curve. These parameters represent the stress relaxation and flexibility of the asphalt at low temperatures, respectively, and are used to assess the crack resistance of the asphalt under cold conditions[2]. To prepare the specimens, the molten asphalt was poured into molds, cooled, and demolded to obtain test specimens with dimensions of 127 mm × 12.7 mm × 6.35 mm. Based on the actual low-temperature conditions along the road, three test temperatures of -12 °C, -18 °C, and -24 °C were selected for this study.

## 2.5 Chemical mechanisms

The changes in the morphological and rheological properties of SBSMA during aging are rooted in alterations in the internal chemical composition and microstructure of the asphalt binder. To elucidate the chemical mechanisms underlying these performance variations, a series of characterization techniques was employed in this study to analyze the evolution of chemical components, molecular distribution, and functional groups of SBSMA under the two aging modes.

### 2.5.1 Functional groups

Fourier transform infrared spectroscopy (FT-IR) was utilized to analyze the alterations in the types and quantities of functional groups within the asphalt binder during the aging process. In accordance with JTG 3410-2025, a Fourier transform infrared spectrometer equipped with an attenuated total reflectance accessory (Thermo Fisher Scientific, Nicolet iS50, USA) was employed. Spectra were acquired over the 4000–400 $cm^{-1}$ range at a resolution of 4 $cm^{-1}$, 64 scans per sample, with the clean diamond crystal serving as the background reference.

The characteristic peak areas of carbonyl (C=O) at 1700 $cm^{-1}$ and sulfoxide (S=O) at 1030 $cm^{-1}$ were selected for analysis, as they are significantly influenced by asphalt aging. Conversely, the peaks at 1450 $cm^{-1}$ and 1375 $cm^{-1}$, corresponding to the bending vibrations of aliphatic C–H, were used as reference peaks due to their relative stability during the aging process. Furthermore, the characteristic peaks of polybutadiene (PB) and polystyrene (PS) segments in SBSMA were identified near 960 $cm^{-1}$ and 690 $cm^{-1}$, respectively. Given that the PB segment contains unsaturated C=C double bonds, which

are highly sensitive to aging and relatively unaffected by other asphalt components, it was selected to evaluate the polymer content in SBSMA[41–43]. A semi-quantitative area calculation method was adopted, wherein the variations in functional groups of SBSMA during aging were quantified by calculating the ratios of the characteristic peak areas to the reference peak areas, as defined by Eqs. (8)–(10).

$$I_{C=O} = \frac{A_{1700\text{cm}^{-1}}}{A_{1375\text{cm}^{-1}} + A_{1450\text{cm}^{-1}}} \tag{8}$$

$$I_{S=O} = \frac{A_{1030\text{cm}^{-1}}}{A_{1375\text{cm}^{-1}} + A_{1450\text{cm}^{-1}}} \tag{9}$$

$$I_{PB} = \frac{A_{960\text{cm}^{-1}}}{A_{1375\text{cm}^{-1}} + A_{1450\text{cm}^{-1}}} \tag{10}$$

Where $I_{C=O}$ and $I_{S=O}$ denote the carbonyl and sulfoxide indices; $I_{PB}$ represents the polybutadiene index; $A_{1700\text{cm}^{-1}}$, $A_{1030\text{cm}^{-1}}$ and $A_{960\text{cm}^{-1}}$ correspond to the peak areas of C=O, S=O, and PB, respectively.

### 2.5.2 Molecular weight

Asphalt is a highly complex fluid containing $10^5$ to $10^6$ distinct molecular species. Asphalt aging is typically accompanied by chemical reactions, such as recombination and oxidation, which promote the transformation of smaller molecules into larger ones. This evolution significantly strengthens intermolecular interactions, contributing to the macroscopic hardening of the binder[34,43]. To characterize the evolution of the molecular weight (MW) distribution during aging, a gel permeation chromatograph (Agilent 1260 Infinity II, USA) was used. Specifically, 10 mg of each asphalt specimen was dissolved in 5 mL of chromatographic-grade tetrahydrofuran for 30 min. The solution was then filtered through a 0.22 μm membrane before injection. The analysis was conducted at a flow rate of 1 mL/min over a 30-min duration with the column oven maintained at 30 °C. Polystyrene was employed as the calibration standard.

The representative chromatogram of asphalt is shown in Fig.4. Asphalt components are categorized into large (LMS), medium (MMS), and small (SMS) molecular sizes based on their elution times. The classification process is as follows: (1) the peak elution time ($P_t$) serves as the threshold between MMS and SMS; (2) the LMS boundary ($L_t$ ) is determined from the total elution

time ($T_t$), which equals the end time ($E_t$) minus the start time ($S_t$) [15,17].

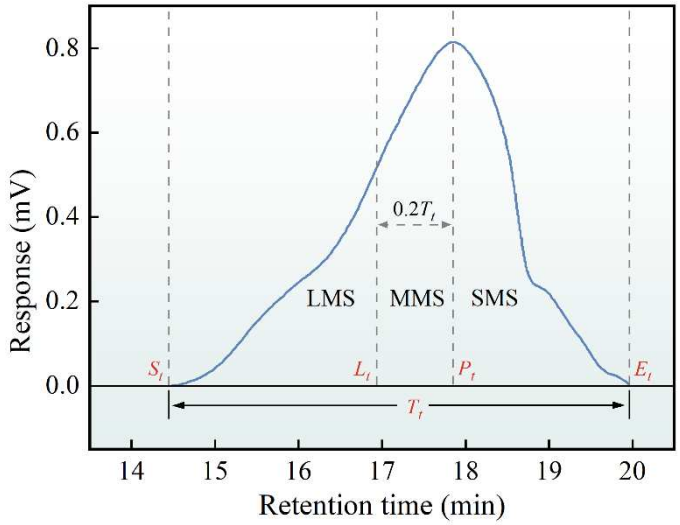



**Fig 4. GPC plot of asphalt**

$$L_t = P_t - 0.2T_t \tag{11}$$

The proportions of LMS, MMS, and SMS were calculated by integrating the GPC curve using Origin software. Furthermore, the weight-average molecular weight ($M_w$), number-average molecular weight ($M_n$), and polydispersity index ($PDI$) were calculated for quantitative characterization using the following equations:

$$M_w = \frac{\sum M_i^2 \times N_i}{\sum M_i \times N_i} \tag{12}$$

$$M_n = \frac{\sum M_i \times N_i}{\sum N_i} \tag{13}$$

$$PDI = \frac{M_w}{M_n} \tag{14}$$

Where $M_i$ and $N_i$ denote the molecular weight and the number of polymer molecules with molecular weight $M_i$, respectively.

### 2.5.3 SARA fractions

Asphalt is a complex mixture whose molecular structure has not yet been fully determined. SARA analysis is a widely accepted standard for categorizing asphalt based on polarity and solubility, which fractionates the binder into saturates, aromatics, resins, and asphaltenes, with varying proportions significantly influencing the material's properties[9,44]. As SBSMA performance

inherently depends on the evolution of these chemical constituents during aging, quantitative analysis of SARA fractions serves to bridge the gap between microscopic molecular transformations and macroscopic performance degradation. In this study, the SARA analysis was performed using thin-layer chromatography with flame ionization detection (TLC-FID) in accordance with the JTG 3410-2025. This technique ionizes the asphalt components through hydrogen flame combustion, measures the resulting ionic current, and records the chromatogram to determine the SARA fractions[45]. A typical TLC-FID chromatogram is illustrated in Fig.5.

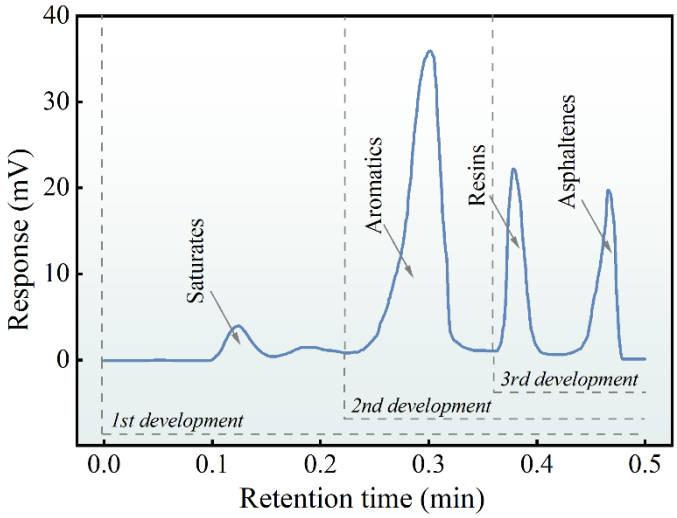



**Fig 5. TLC-FID Chromatogram of Asphalt Four Components**

To quantify the evolution of colloidal stability during the aging process, the colloidal instability index ($I_C$) was determined. Depending on the relative distribution of the four fractions, the asphalt colloidal structure is generally categorized as sol, sol-gel, or gel. An increasing $I_C$ signifies a transition towards a gel-type colloidal structure, which implies reduced stability and increased susceptibility to performance deterioration upon aging[11]. The $I_C$ is defined as follows:

$$I_C = \frac{A_{sat} + A_{asp}}{A_{aro} + A_{res}} \tag{15}$$

Where $A_{sat}$, $A_{asp}$, $A_{aro}$, and $A_{res}$ represent the mass fractions of saturates, asphaltenes, aromatics, and resins in the binder, respectively.

## 2.6 Statistical analysis

HCA was employed to reveal the internal grouping structure of the multi-indicator system by

iteratively merging indicators based on the similarity of their evolutionary trends[46,47]. Data across five aging intervals, 7, 20, 60, 120, and 180 days, constituted the sample set. The Pearson correlation coefficient was used to construct the similarity matrix to quantify the linear associations among indicator evolutions. Concurrently, SRCA was applied to evaluate monotonic relationships between microscopic mechanism indicators and rheological performance, which is suitable for small sample size and non parametric conditions. The two correlation methods showed consistent trends in the direction of variable associations. The formulation is expressed as:

$$r(i,j)=\frac{\sum_{k=1}^{n}\left(x_{ik}-\bar{x}_i\right)\left(x_{jk}-\bar{x}_j\right)}{\sqrt{\sum_{k=1}^{n}\left(x_{ik}-\bar{x}_i\right)^2}\sqrt{\sum_{k=1}^{n}\left(x_{jk}-\bar{x}_j\right)^2}} \tag{16}$$

$$d(i,j)=1-r(i,j) \tag{17}$$

Where $x_{ik}$ denotes the value of indicator $i$ at the $k$-th aging time point，$\bar{x}_i$ is its mean, and $n$ = 5. A value of $d$ approaching 0 indicates a high degree of synchronization in the evolutionary trends of two indicators, while a value approaching 2 suggests opposite trends.

The Ward's minimum variance method was utilized for cluster merging to achieve data grouping by minimizing intra-cluster variance, with the formula as follows:

$$\Delta ESS_{pq}=\frac{n_p n_q}{n_p+n_q}\left\|\bar{x}_p-\bar{x}_q\right\|^2 \tag{18}$$

Where $n_p$ and $n_q$ represent the capacities of the two clusters to be merged, $\bar{x}_p$, $\bar{x}_q$ denote their respective centroids.

The optimal number of clusters was determined based on the maximum jump in merge distance; when a significant order-of-magnitude increase in the merge distance was observed, the clustering process was truncated prior to that step.

SRCA was further performed to establish associations between microscopic mechanism indicators and macroscopic rheological performance. This method solely characterizes the monotonic synchronization between two variables, making it more suitable for the small-sample monotonic aging time series in this study.

$$\rho=1-\frac{6\sum_{k=1}^{n}d_k^2}{n(n^2-1)} \tag{19}$$

Where $d_k$ is the difference in rank between the two variables at the $k$-th aging node, and $n = 5$.

The magnitude and sign of $\rho$ characterize the strength and direction of the association between variables, with $\rho$ approaching ±1 indicating a perfectly monotonic positive or negative correlation, respectively.

# 3 Results and analysis

## 3.1 Morphological evolution

### 3.1.1 Visual and SEM analysis

The surface morphologies of SBSMA at different aging intervals are presented in Fig.6. The virgin and short term aged specimens exhibit smooth and lustrous surfaces. Under both aging modes, a gray aged film gradually forms with increasing aging time, accompanied by loss of luster and increasingly irregular surface textures. This could explained by the progressive accumulation of oxidation products and localized separation between the SBS modifier and asphalt matrix.

The two aging modes appear to produce different crack development characteristics. For the specimens aged under UVA, the surface becomes progressively rough and wrinkled, but no extensive cracks are macroscopically visible even after 180 days of aging. At the microscopic scale, the cracks remain shallow and are mainly confined to the aged surface film, while the underlying binder shows comparatively limited deterioration. Under CPA, however, cracks progressively develop into an extensive network by day 180. These cracks are denser and appear to penetrate more deeply into the underlying binder, suggesting more pronounced subsurface deterioration. This difference may be attributed to temperature fluctuations that promote crack initiation and propagation. Therefore, although both aging modes cause surface roughening and apparent phase separation, CPA is likely to induce more severe cracking and surface deterioration.

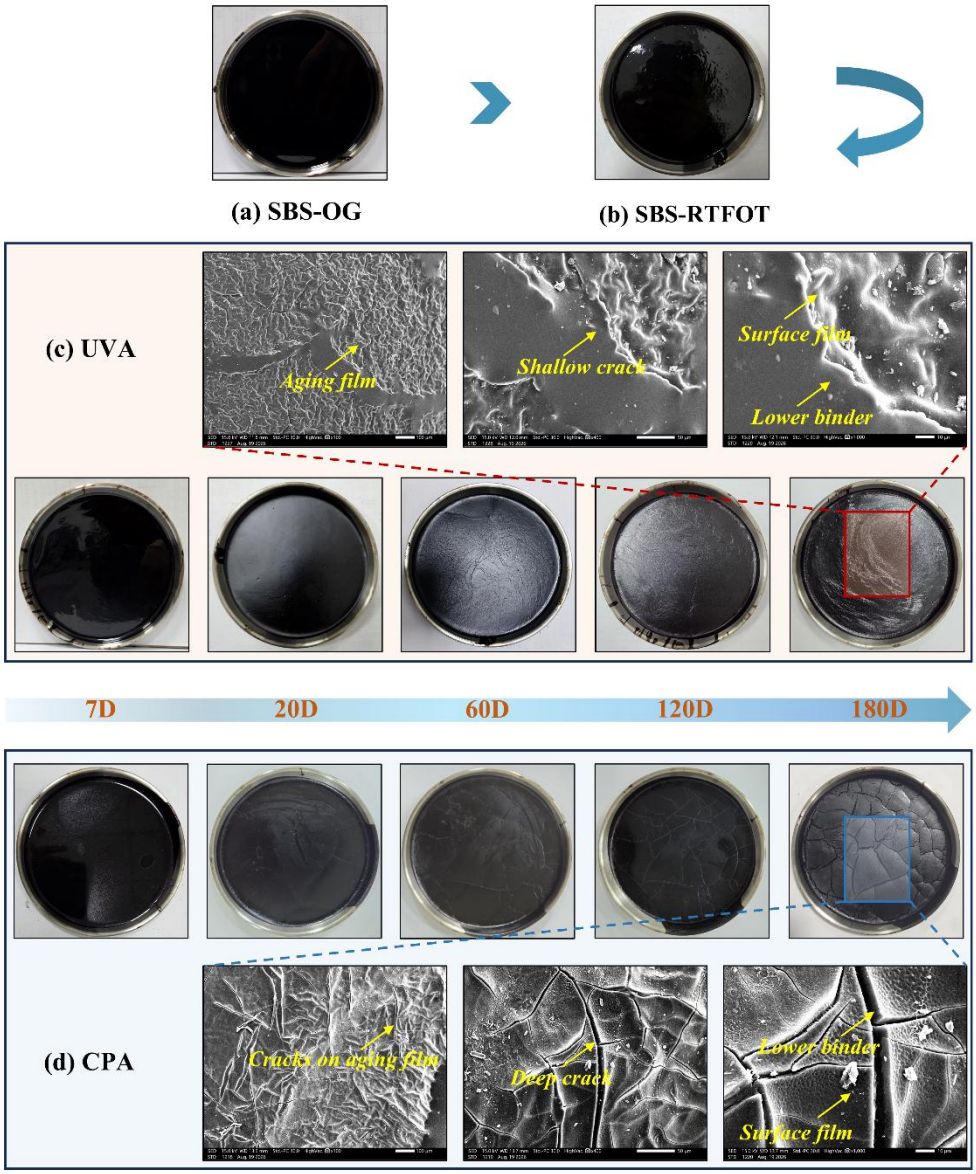



**Fig 6. Surface evolution of SBSMA samples under the two aging modes**

### 3.1.2 FM analysis

The morphological evolution of SBS in SBSMA under UVA and CPA was observed by FM, and the fluorescence images are presented in Fig.7. After short term aging, the fluorescence intensity of SBSMA decreased slightly, while a certain reticulated structure was still maintained, indicating that the polymer network in SBSMA was not effectively destroyed at this stage. With the prolongation of UV aging, the fluorescent regions in both UVA and CPA samples gradually decreased, showing a similar overall degradation trend. At the early aging stage, the continuous polymer network gradually fractured into interlaced filamentous structures. After 120 days of aging, large areas of the polymer phase disappeared, and the degraded polymer fragments were dispersed or dissolved in the asphalt

matrix. After 180 days of aging, the reticulated polymer structure was almost invisible, with only isolated polymer particles or fragments remaining. This phenomenon suggests that SBS had undergone severe degradation after long-term UV exposure.

To quantify the degree of degradation of SBS during the aging process, the $I_{SBS}$ of each aged sample was calculated, and the results are shown in Fig.8. As shown in the figure, the SBS content of SBSMA continuously decreased under both UVA and CPA conditions, consistent with the trends observed in the images. Specifically, the $I_{SBS}$ of the CPA samples decreased sharply from day 7 to day 60, whereas the rapid decline of $I_{SBS}$ for the UVA samples was delayed to the period from day 20 to day 120. The reduction in $I_{SBS}$ during these two stages accounted for 67.9% and 68.8% of their respective entire degradation processes, indicating that these two periods represent the primary stages of SBS degradation in SBSMA under the two aging modes, and that SBS degradation initiates earlier under CPA. By day 180 of aging, the $I_{SBS}$ of the CPA sample was only 16.72%, which was 36.80% of that of the unaged asphalt, and was 5.56% lower than that of the UVA sample at the same aging duration. This indicates that under long-term exposure, CPA exerts a more severe degradation effect on SBS than UVA. Observation of the slope curves of SBS content change reveals that SBS degradation under both UVA and CPA exhibited a trend of initial acceleration followed by deceleration. The inflection points where the degradation rates under UVA and CPA slowed down significantly occurred on day 120 and day 60, respectively. This demonstrates that CPA not only intensifies the degradation of SBS in SBSMA in the long term, but also accelerates SBS degradation in the short term.

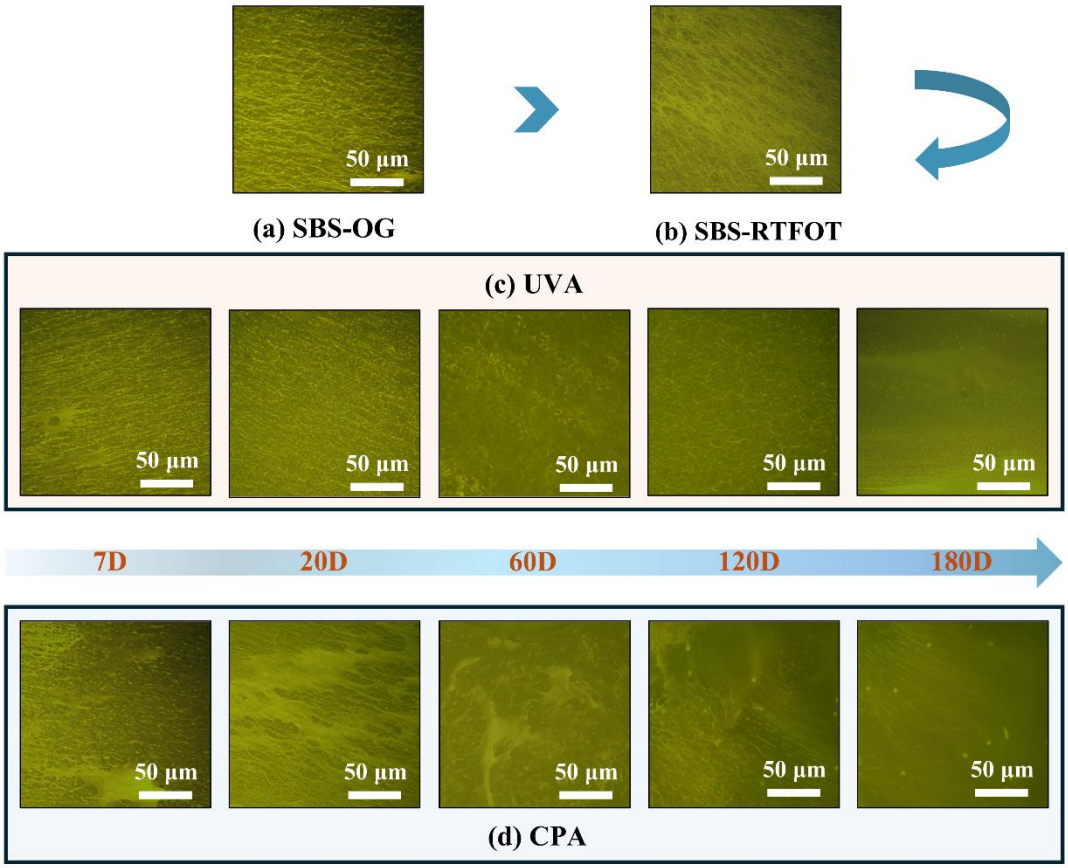



Fig 7. Fluorescence images of SBSMA under the two aging modes

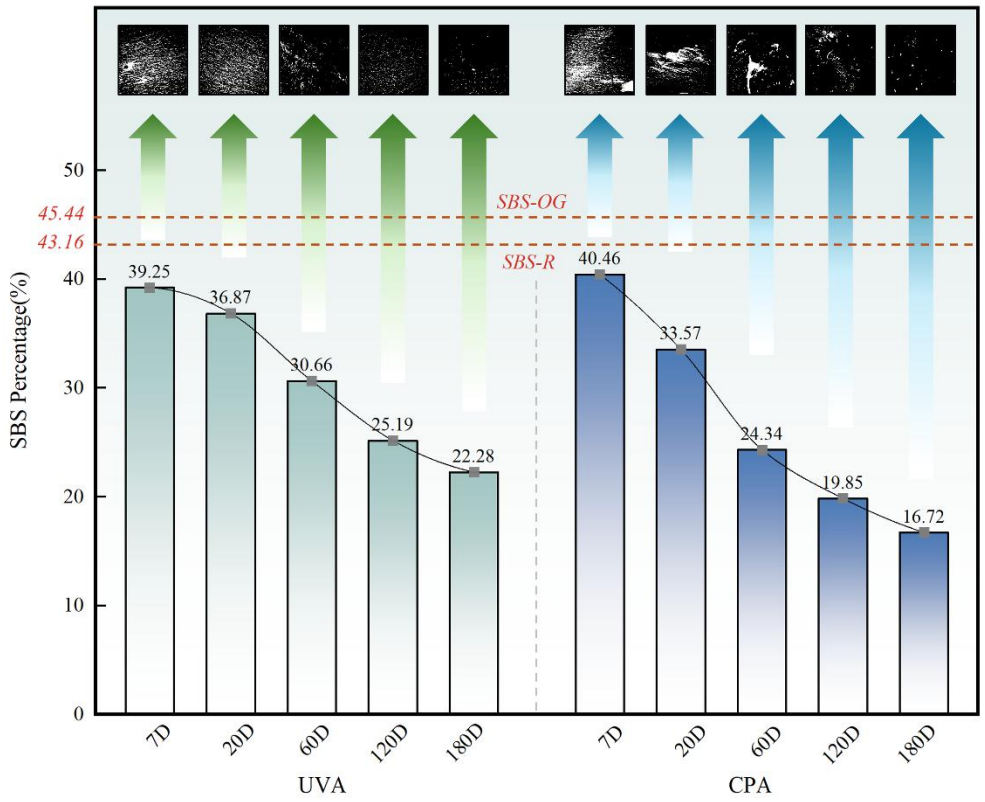



Fig 8. $I_{SBS}$ of SBSMA under the two aging modes

### 3.1.3 AFM analysis

The microstructure of the aged SBSMA surface is shown in Fig.9. Distinct "bee-like" structures could be observed on the surface of all samples, which is generally considered to be related to the aggregation of asphaltenes in asphalt[15,20,34]. For virginal and short-term aged specimens, these bee-like structures were fine, densely distributed, and uniform in size. As the aging duration extended, both UVA- and CPA-aged specimens exhibited a reduction in the density of these structures accompanied by an increase in their individual areas, likely due to the UV-promoted coalescence of asphaltene molecules. Notably, between 120 and 180 days of CPA, the area of these bee-like structures decreased and eventually dissipated. This phenomenon suggests that under prolonged CPA, the repeated thermal stresses induce the initiation and propagation of micro-cracks on the surface. Coupled with the phase separation of SBS, these mechanisms disrupt the originally orderly bee-like structures, leading to a more complex and irregular surface morphology at the micro-scale.

The surface roughness parameters, $R_q$ and $R_a$, were calculated and are summarized in Tab 3. Throughout the aging process, the CPA specimens consistently exhibited higher roughness values than the UVA specimens, reflecting their more irregular and heterogeneous surface characteristics. For the UVA-aged specimens, both $R_q$ and $R_a$ decreased continuously with aging time. By day 180, the $R_q$ and $R_a$ of UVA-180D specimens were below 2 nm, representing only 63.2% and 62.9% of the values for the pristine binder, respectively. This decline indicates a continuous reduction in surface roughness, as the aggregation and coalescence of asphaltenes under UV radiation enlarge the bee-like structures and merge small peaks, thereby reducing the peak-valley height difference and smoothing the overall surface. In contrast, the surface roughness of the CPA-aged specimens followed a non-monotonic trend, characterized by an initial decrease followed by a subsequent rise. In the early stage of aging, the surface $R_q$ and $R_a$ of CPA specimens continuously decreased, reaching their lowest values on day 20; the $R_q$ and $R_a$ of the CPA-20D specimen were 3.064 nm and 1.978 nm, respectively, at which point asphaltenes were continuously aggregating. Subsequently, the surface roughness increased sharply; the $R_q$ and $R_a$ of the CPA-60D specimen had increased to 3.944 nm and 2.891 nm, respectively, exceeding the SBS-R level. With further aging, the repeated action of thermal stress promoted the initiation and propagation of surface microcracks, further increasing the irregularity of the aged asphalt surface. The $R_q$ and $R_a$ of the CPA-180D specimen reached 6.615 nm and 5.621 nm, respectively, representing increases of 109.1% and 173% compared with unaged asphalt, indicating

that under long-term CPA, the surface microstructure of aged SBSMA underwent significant changes distinct from those under UVA.

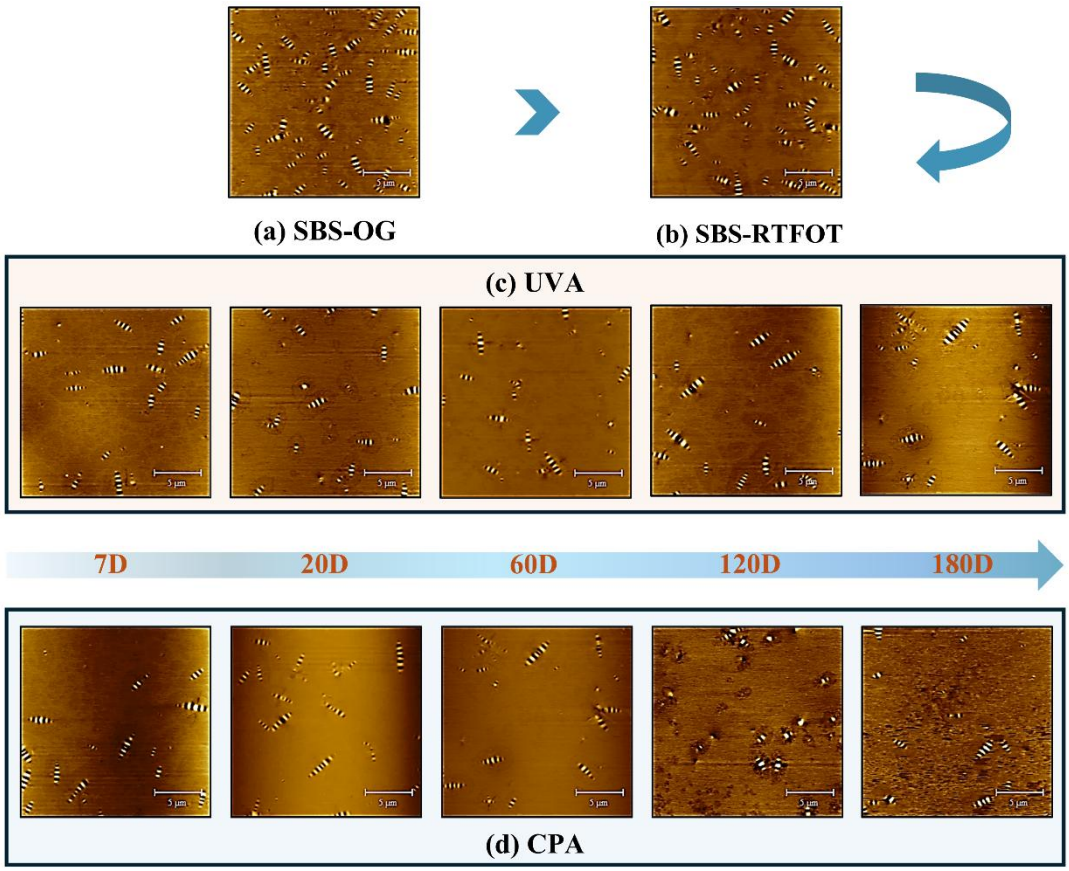



**Fig 9. AFM images of SBSMA under the two aging modes**

**Tab 3. $R_a$ and $R_q$ results of SBSMA under the two aging modes**

| Index | $R_q$(nm) | $R_a$(nm) | $R_q$(nm) | $R_a$(nm) |
|---|---|---|---|---|
| Condition | UVA | | CPA | |
| SBS-OG | 3.163 | 2.058 | 3.163 | 2.058 |
| SBS-R | 3.395 | 2.100 | 3.395 | 2.100 |
| 7D | 2.947 | 1.866 | 3.252 | 2.049 |
| 20D | 2.461 | 1.520 | 3.064 | 1.978 |
| 60D | 2.217 | 1.385 | 3.944 | 2.891 |
| 120D | 2.164 | 1.342 | 4.353 | 3.429 |
| 180D | 1.998 | 1.296 | 6.615 | 5.621 |

## 3.2 Rheological properties

### 3.2.1 TS analysis

Temperature sweep tests were conducted on the SBSMA specimens under the two aging modes

to obtain $G^*$ and $\delta$. $G^*$ reflects the overall resistance to shear deformation, whereas $\delta$ represents the phase difference between the stress and strain responses under sinusoidal loading and indicates the relative proportions of the viscous and elastic components. As shown in Fig.10, after the increase in $G^*$ induced by short-term thermo-oxidative aging, UV aging further raised the overall $G^*$ of the SBSMA, thereby enhancing its resistance to shear deformation. In terms of the phase angle, the SBSMA exhibited a plateau in the $\delta$ curve over 64–76 °C in both the unaged and short-term thermo-oxidatively aged states, within which $\delta$ decreased with increasing temperature, reflecting the dominant elastic contribution of the polymer network at high temperatures[36]. With the onset and progression of UV aging, these plateaus gradually disappeared in both the UVA and CPA samples, and $\delta$ increased continuously at high temperatures. This indicates the degradation of the polymer network and an increase in the proportion of viscous components, which consequently led to greater plastic deformation of the aged SBSMA at high temperatures.

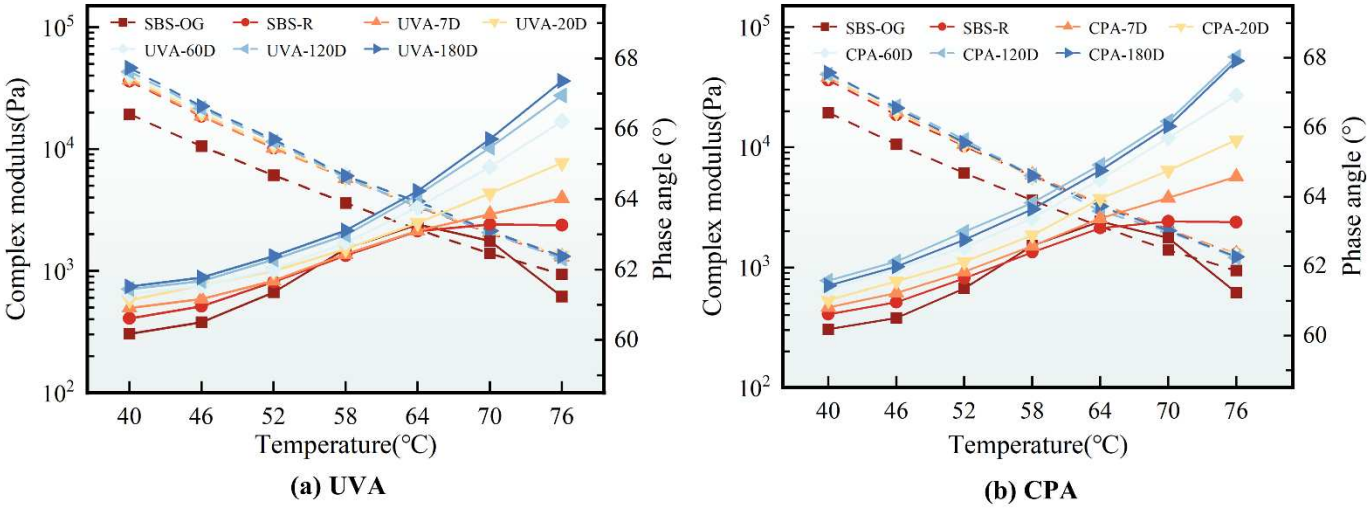



**Fig 10. Complex modulus and phase angle of SBSMA under the two aging modes**

To accurately analyze the evolution of the high-temperature rheological properties, the $G^*$ and $\delta$ of the aged binders at 70 °C were used to calculate the aging indices $AI_{CM}$ and $AI_{PA}$, as shown in Fig.11. The $AI_{CM}$ of both the UVA and CPA samples first decreased and then increased. Specifically, the $AI_{CM}$ under UVA rebounded markedly after 120 days of aging, whereas that under CPA began to rise continuously from day 7. This variation in $AI_{CM}$ differs from the conventional finding that asphalt aging leads to a monotonic increase in $G^*$. The aging of SBSMA results from the competition between the photo-oxidative hardening of the asphalt matrix and the degradation of the SBS polymer. Photo-oxidation induces hardening and raises $G^*$, whereas SBS degradation weakens the reinforcing

contribution of the polymer and thus lowers $G^*$ [48,49]. The relative dominance of these two effects at different stages determines the net change in $G^*$. When SBS degradation dominates, $G^*$ decreases, and when photo-oxidation dominates, $G^*$ increases. Accordingly, it is inferred that, for CPA, SBS degradation dominated the early aging stage, whereas asphalt hardening became dominant after day 60. For UVA, this transition from degradation-dominated to oxidation-dominated aging was delayed to day 120. Combined with the morphological analysis, this transition corresponds to the extensive disruption of the SBS network, suggesting that the CPA mode markedly accelerates the degradation of SBS. Furthermore, the $AI_{CM}$ of the UVA and CPA samples was generally lower than that of the thermo-oxidatively aged samples, because the adverse effect of SBS degradation on the resistance to shear deformation outweighed the positive hardening effect of the asphalt matrix at 70 °C. By day 180, the $AI_{CM}$ of the CPA-180D sample was 47.1 %, slightly lower than the 47.6 % of the UVA-180D sample, indicating that the high-temperature deformation resistance of the UVA sample was slightly superior to that of the CPA sample under long-term aging. The origin of this difference will be elucidated in the subsequent sections.

The $\delta$ of the aged SBSMA was likewise governed by both SBS degradation and asphalt hardening. SBS degradation reduces the elastic polymer content and raises $\delta$, whereas oxidation hardens the asphalt and lowers $\delta$. The $AI_{PA}$ under both UVA and CPA increased throughout the aging process, reaching 4.28 % and 4.41 %, respectively, by day 180. Both aging modes exhibited an $AI_{PA}$ growth that was rapid at first and then slowed, with transition points at day 120 and day 60, respectively, corresponding to the time required for sufficient degradation of the SBS network in each sample group. The analysis suggests that, in the early stage, the variation in $\delta$ is primarily driven by SBS degradation, which leads to continuous softening of the asphalt and a rapid increase in $\delta$. Beyond the transition point, although aging becomes dominated by asphalt oxidation, $\delta$ remains sensitive to SBS degradation at high temperatures. Consequently, the rise in $\delta$ driven by SBS degradation outweighs the suppression caused by asphalt hardening, resulting in a continuous net increase in the phase angle.

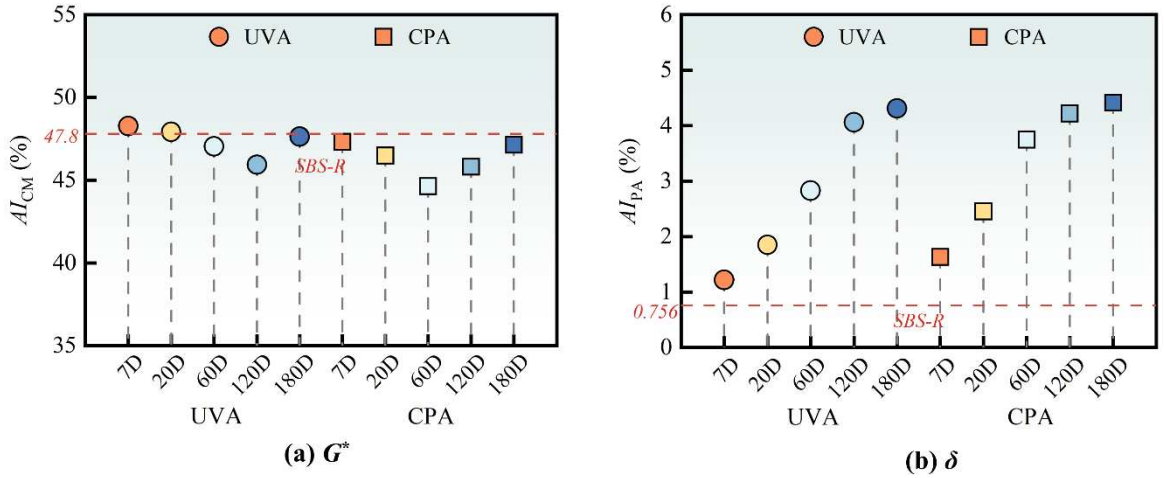



**Fig 11. Aging index of complex modulus and phase angle of SBSMA under the two aging modes**

### 3.2.2 MSCR analysis

The MSCR test was employed to further evaluate the viscoelastic properties of aged SBSMA, and the results are shown in Fig.12. *R* characterizes the elastic response of the binder, where a higher value indicates superior elasticity; $J_{nr}$ reflects the resistance to high-temperature deformation, where a higher value signifies greater non-recoverable deformation and poorer resistance to permanent deformation[36]. Under both aging conditions, $J_{nr}$ at the high stress level is larger than that at the low stress level, and *R* is smaller than that at the low stress level, indicating that the aged SBSMA exhibits larger non-recoverable deformation and weaker elastic recovery capability under heavy load conditions.

The variation in *R* shows that the elastic recovery rate of SBSMA continuously decreased with aging time under both UVA and CPA. This is because *R* reflects the elastic recovery ability of polymer chain segments in SBSMA, which mainly depends on the integrity of the SBS network. As SBS undergoes oxidative chain scission under UV irradiation, its elastic network is irreversibly damaged, resulting in a monotonic decrease in *R* throughout the aging period. Compared with UVA, CPA caused a much faster decline in *R*. After 60 days of aging, *R* of the CPA-60D sample at the low stress level decreased to approximately 15%, whereas that of the UVA-60D sample remained at approximately 47%. This confirms that the coupled action of UV radiation and temperature variation accelerated the decomposition of the SBS elastic network.

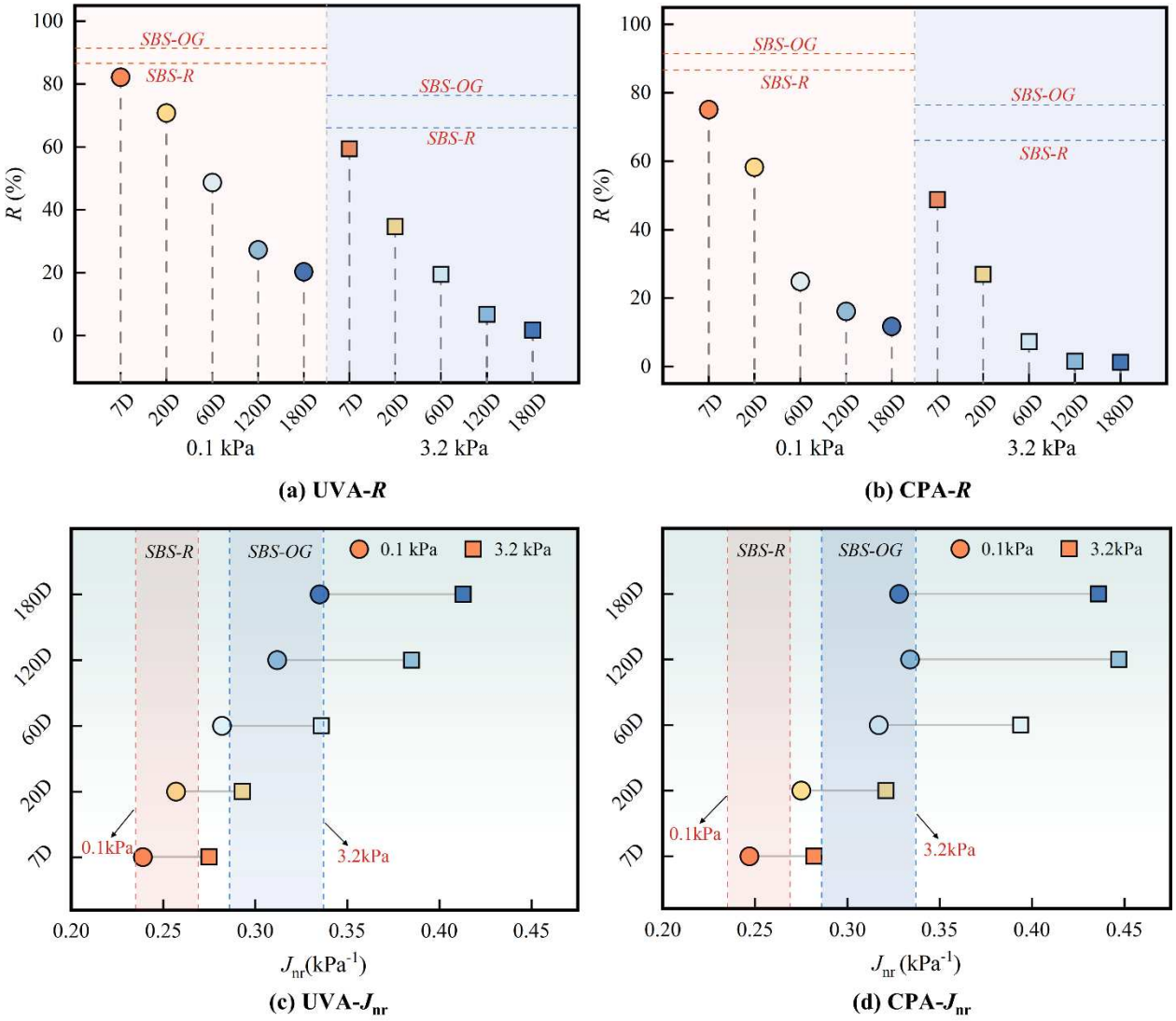



**Fig 12. MSCR results of SBSMA under the two aging modes**

Due to the different relative rates of SBS degradation and asphalt oxidation under UVA and CPA, the evolution of $J_{nr}$ exhibited distinct patterns. Under UVA, $J_{nr}$ increased continuously with aging time, indicating that the beneficial effect of asphalt oxidation on deformation resistance was offset by SBS degradation, leading to an overall reduction in resistance to permanent deformation. Under CPA, $J_{nr}$ showed a staged trend, first increasing and then decreasing. From 7 to 60 day, rapid SBS degradation weakened the contribution of SBS to deformation resistance, causing a sharp increase in $J_{nr}$. After 120 days of aging, as SBS had been extensively degraded, asphalt hardening gradually became dominant and slightly reduced $J_{nr}$. Nevertheless, the $J_{nr}$ of the CPA-180D sample at both high and low stress levels remained higher than those of the corresponding UVA samples, demonstrating that coupled aging induced by intense UV radiation and large temperature variation had a much more

589 detrimental effect on the high temperature deformation resistance of SBSMA than single UV aging.

590 **3.2.3 LAS analysis**

591 LAS tests were conducted on aged SBSMA at strain levels of 5%, 10%, and 15%, and the fatigue
592 life of aged binders was predicted based on the VECD model. The results are shown in Fig.13. It can
593 be observed that the fatigue life $N_f$ of SBSMA decreased monotonically with aging time under both
594 UVA and CPA, indicating that aging continuously weakened the fatigue resistance of SBSMA. At all
595 aging stages, the fatigue life followed the order of 5% > 10% > 15%, suggesting that a higher strain
596 amplitude resulted in a shorter $N_f$. Moreover, at the high strain level of 15%, the difference in $N_f$
597 between UVA and CPA samples at the same aging duration became more pronounced, indicating that
598 the difference between the two aging modes in deteriorating the fatigue resistance of SBSMA was
599 more evident under high strain conditions.

600 The evolution of $N_f$ under UVA and CPA further reveals the different fatigue deterioration
601 processes induced by the two aging modes. In terms of the rate of $N_f$ reduction, a marked decrease in
602 $N_f$ under UVA mainly occurred from day 20 to day 120, whereas the rapid attenuation of $N_f$ under
603 CPA was concentrated from day 7 to day 60. These periods corresponded well to the main degradation
604 stages of SBS under the two aging modes, indicating that SBS degradation was an important factor
605 responsible for the rapid deterioration of the fatigue resistance of SBSMA during aging. At the later
606 aging stage, the $N_f$ values of CPA samples were significantly lower than those of UVA samples with
607 the same aging duration. At the strain level of 15%, the $N_f$ of CPA-180D was only $1.09 \times 10^2$ cycles,
608 corresponding to approximately 39.1% of that of UVA-180D. At the medium and low strain levels of
609 10% and 5%, the corresponding ratios were only 62.3% and 76.7%, respectively. These results
610 demonstrate that long-term CPA reduced the fatigue life of aged SBSMA more severely than UVA.
611 In addition to accelerated SBS degradation and asphalt oxidation, repeated thermal stress generated
612 inside SBSMA during large temperature variation cycles may further accumulate microscopic
613 damage, thereby causing an additional reduction in $N_f$ under CPA.

614

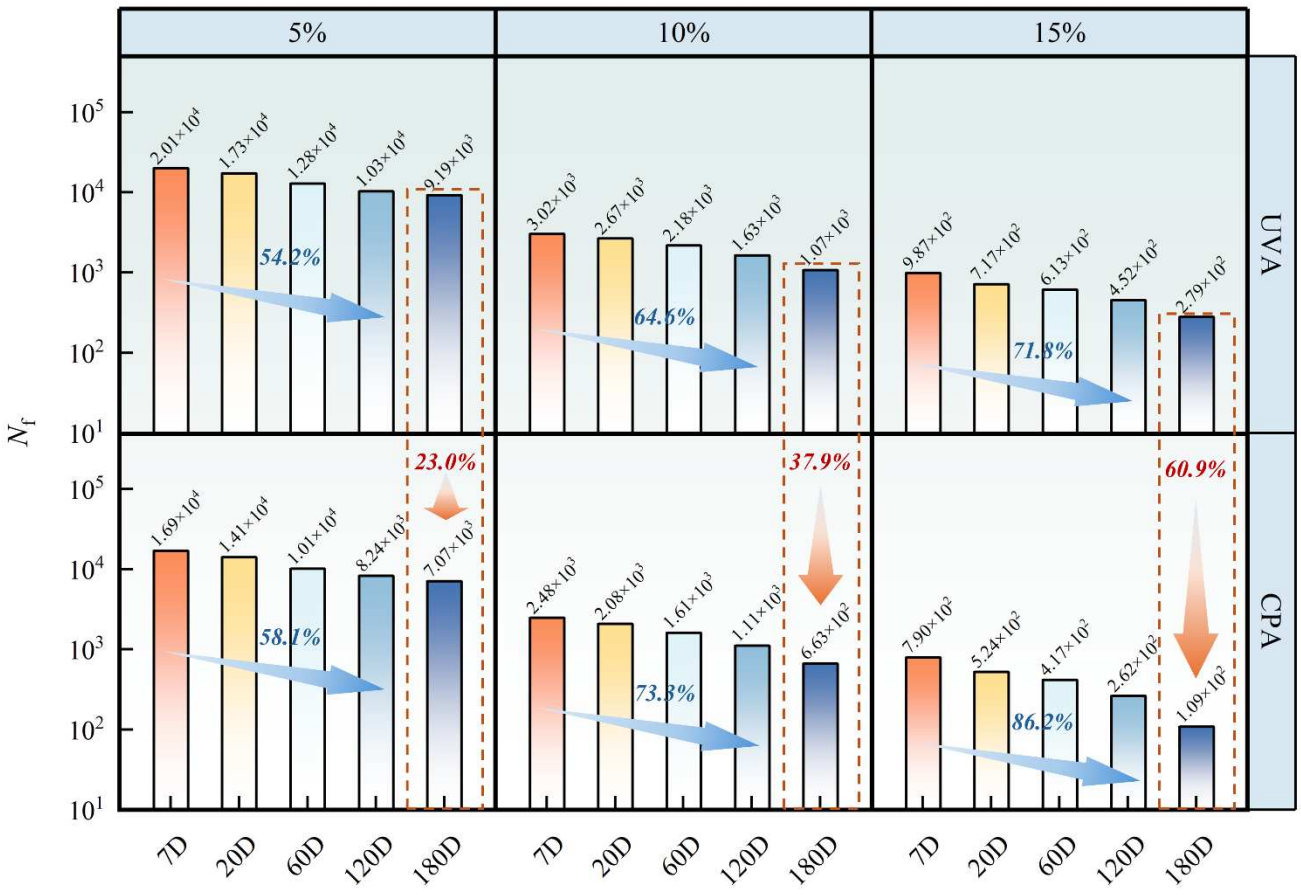



**Fig 13. Fatigue life of SBSMA under the two aging modes**

### 3.2.4 BBR analysis

The BBR test evaluates the stress relaxation and flexible deformation capacity of asphalt at low temperature by measuring the creep stiffness *S* and creep rate *m* of asphalt beams. A higher *S-value* indicates that the binder is stiffer and has weaker deformation capacity at low temperature, whereas a higher *m-value* indicates stronger stress relaxation ability and better crack resistance[2]. The BBR results of samples under the two aging modes are shown in Fig.14. With decreasing test temperature and prolonged aging time, the *S-value* of all aged SBSMA samples continuously increased, whereas the m value continuously decreased. This indicates that both temperature reduction and aging aggravation significantly weakened the deformation capacity of aged SBSMA. At -12 °C, the *S-*values of all aged samples at different aging stages were lower than 300 MPa, and the *m-values* were higher than 0.3, satisfying the technical requirements of AASHTO M320 for PG 70-22 binders. At -18 °C, the samples aged for no more than 60 days still met the specification requirements. When the aging time increased to 120 days, the *m-values* of both UVA and CPA samples decreased below 0.3,

indicating that the stress relaxation ability of the aged binders could no longer meet the specification requirement. When the test temperature further decreased to -24 °C, the *m* value of UVA-120D was 0.237, which was lower than the limiting value of 0.3, suggesting insufficient relaxation capacity under low temperature conditions. Under CPA, the *S-value* of CPA-60D already reached 312.8 MPa, and its *m-value* was 0.287, failing both technical requirements. This indicates that the coupled action of intense UV radiation and large temperature variation accelerated and intensified the deterioration of the deformation performance of SBSMA at low temperature.

At the same aging duration and test temperature, the *S-value* of CPA samples was consistently higher than that of UVA samples, whereas the *m-value* was consistently lower, indicating that CPA caused a much more severe deterioration the deformation of aged SBSMA than UVA. Taking 180 days of aging as an example, at 24 °C below zero, the *S-value* of CPA-180D reached 474.0 MPa, which was much higher than the 388.3 MPa of UVA-180D. The *m-value* of CPA-180D was 0.227, lower than the 0.235 of UVA-180D. These results indicate that CPA made aged asphalt stiffer and more brittle at low temperatures and further weakened its stress relaxation ability, thereby increasing its cracking susceptibility. The severe deterioration in the relaxation capacity of aged SBSMA under CPA can be attributed to three processes. First, CPA accelerated and intensified SBS degradation, and the substantial loss of elastic SBS components weakened the deformation capacity of SBSMA. Second, asphalt oxidation increased the proportion of heavy components, resulting in higher rigidity. Third, large temperature variation cycles may have induced physical damage within SBSMA, further deteriorating its deformation capacity. It is worth noting that, unlike the high temperature properties of aged SBSMA, which are governed by the competition between SBS degradation and asphalt hardening, SBS degradation, asphalt oxidation and potential physical damage all led to an increase in *S-value*, a decrease in *m-value*, and deterioration of deformation capacity in the low temperature range. This explained why pavement cracking is more prevalent and severe than permanent deformation in the QTP region.

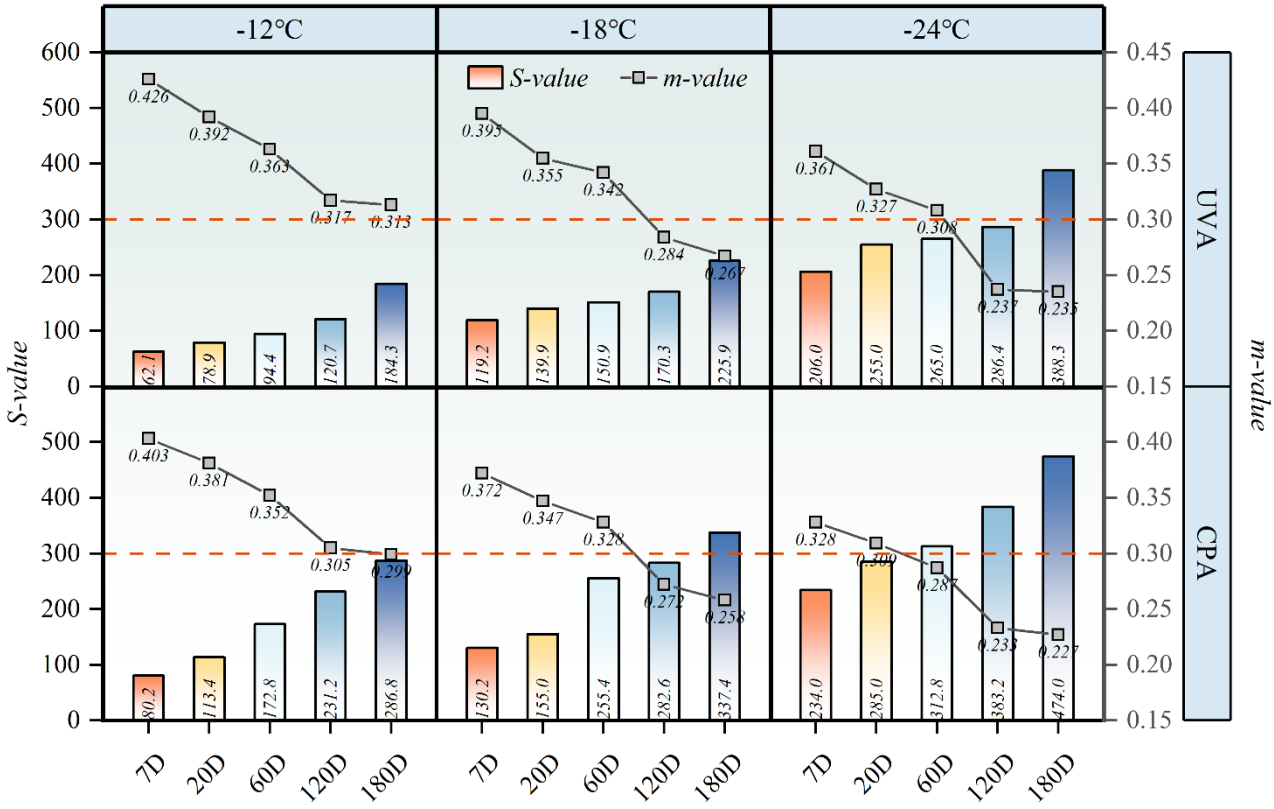



**Fig 14. BBR results of SBSMA under the two aging modes**

## 3.3 Mechanism analysis

### 3.3.1 FT-IR analysis

The FT-IR spectra of SBSMA under the UVA and CPA aging modes are presented in Fig. 15. Overall, the two aging regimes exhibit consistent spectral evolution trends. As the UV aging time increases, the intensity of the characteristic S=O peak at 1030 $cm^{-1}$ rises continuously, indicating that the sulfur-containing components in the binder are oxidized into S=O. The stretching vibration of the C=O at 1700 $cm^{-1}$ appears between day 7 and 20 of aging and intensifies markedly thereafter, suggesting that carbon chain oxidation gradually becomes the dominant reaction and drives the accumulation of oxygen-containing polar functional groups. The characteristic absorption peak of the PB block of SBS at 960 $cm^{-1}$ declines steadily throughout aging, confirming that UV radiation induces continuous chain scission of the butadiene segments and the gradual breakdown of the SBS polymer network. Compared with the CPA samples, the UVA-180D specimen exhibits a new absorption peak at 1260 $cm^{-1}$, which may be ascribed to the C–O–C stretching of deeply oxidized products such as esters or anhydrides[34], implying that SBSMA undergoes more severe oxidation

under long-term UVA exposure.

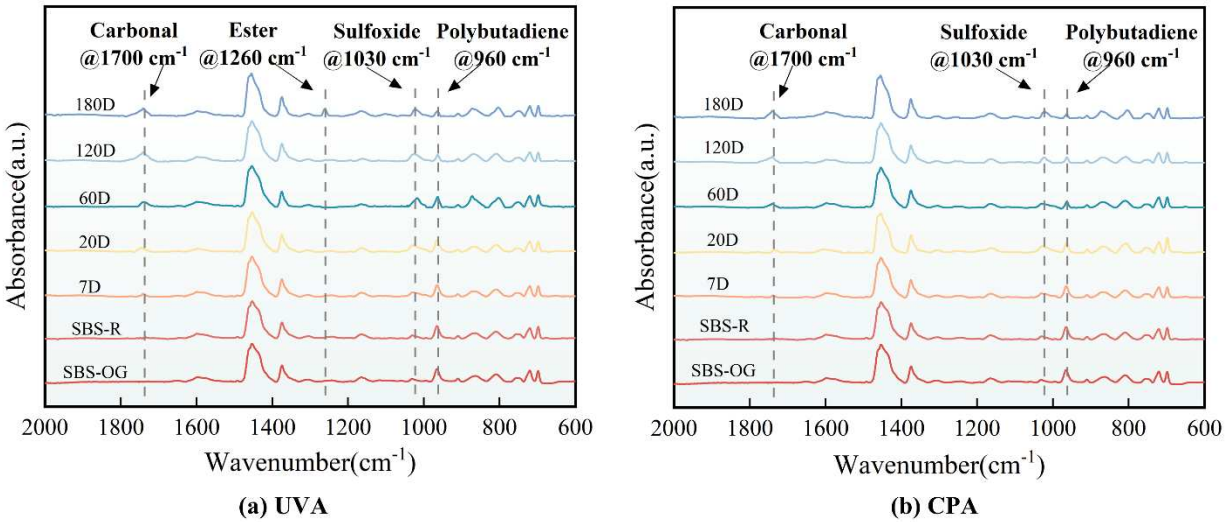



**Fig 15. FT-IR spectra of SBSMA under the two aging modes**

The quantitative results of the functional group indices are further presented in Fig.16. The evolution of these indices displays distinct multi-stage characteristics under both aging conditions. $I_{S=O}$ rises rapidly in the early aging stage and stabilizes around day 60, whereas $I_{C=O}$ increases slowly at first and then accelerates markedly after day 60. This difference arises because sulfur bonds are more reactive than carbon chains, so sulfur atoms preferentially combine with oxygen to form S=O in the early stage, after which carbon chain oxidation becomes dominant and carbonyl accumulate rapidly. Throughout aging, both $I_{S=O}$ and $I_{C=O}$ follow the order UVA > CPA. This indicates that the overall oxidation degree of SBSMA under CPA is lower than that under UVA, most likely because the low-temperature stages of the CPA thermal cycle slow the reaction between oxygen and the internal asphalt molecules, thereby inhibiting oxidation to some extent. This also explains why the $AI_{CM}$ of the CPA-180D sample is slightly lower than that of the UVA-180D sample. As for $I_{PB}$, the UVA samples consistently show higher values than the CPA samples. The $I_{PB}$ of the UVA samples begins to drop markedly on day 20, whereas that of the CPA samples decreases noticeably as early as day 7. By day 180, the $I_{PB}$ of the CPA-180D sample is approximately 8.9 % of that of the SBS-OG sample, compared with 32.4 % for the UVA-180D sample, providing further evidence that CPA aggravates the photo-oxidative degradation of SBS. In summary, the FT-IR results reveal that SBS degradation and asphalt oxidation proceed simultaneously throughout both the UVA and CPA aging processes, with their relative dominance shifting over time. SBS degradation prevails in the early

aging stage, whereas asphalt oxidation becomes the governing mechanism in the later stage.

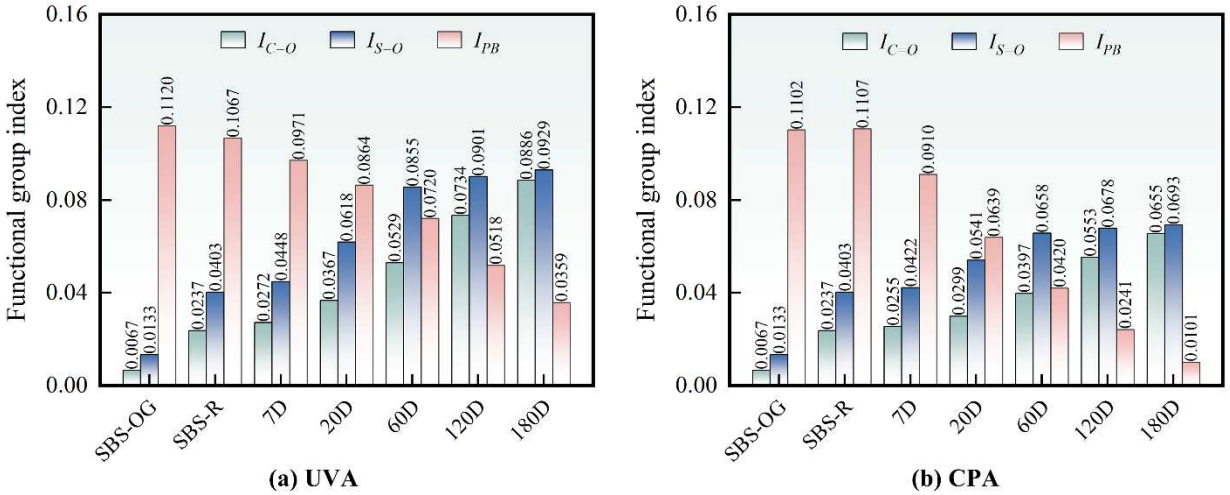



**Fig 16. Functional group indices of SBSMA under the two aging modes**

### 3.3.2 GPC analysis

The molecular weight and its distribution of SBSMA under UVA and CPA aging are presented in Tab.4 and Fig.17. As the aging progresses, both aging modes exhibit a consistent overall trend, in which the LMS proportion increases while the SMS content decreases, accompanied by a continuous increase in $M_n$, $M_w$, and $PDI$. This indicates that aging drives the sustained transformation of the small molecular components into large molecular components within SBSMA, and the system as a whole evolves toward a higher molecular weight and a broader distribution. This is mainly because the light components such as aromatics and resins in the asphalt phase continuously undergo oxidative polycondensation, generating asphaltene-like substances with higher molecular weights and thereby steadily increasing the molecular weight of the system. Meanwhile, the SBS polymer mainly undergoes chain scission under UV radiation, and its high-molecular-weight chains are gradually broken into smaller fragments whose molecular weights approach those of asphaltenes, which reduces the contribution of the polymer to the large-molecule region[48]. However, owing to the relatively low SBS content in the system, the influence of SBS degradation on the molecular weight variation of the asphalt is limited. As a result, the molecular weight evolution of SBSMA is still dominated by asphalt oxidation, and all the indices present monotonic trends.

Specifically, the MW evolution under CPA differs from that of UVA in distinct stages. During the initial aging phase, the LMS proportion in CPA-aged samples is lower than that in UVA-aged

counterparts, accompanied by higher SMS levels and smaller increases in $M_w$ and *PDI*. This suggests that the low-temperature periods within the CPA cycle retard oxidative reactions; furthermore, the fragments generated by SBS degradation may temporarily replenish the small-to-medium molecular weight fractions, thereby slowing the accumulation of large molecules compared to the UVA regime. From 60 to 180 day, as the majority of SBS has degraded, molecular weight changes are predominantly governed by oxidative processes, narrowing the differences in LMS, $M_w$, and *PDI* between the two modes. By day 180, the $M_w$ and *PDI* of the CPA-aged sample are 3754 g/mol and 3.067, respectively, which are slightly lower than the 3898 g/mol and 3.172 observed for the UVA-aged sample. In conclusion, the MW evolution of aged SBSMA results from the synergistic effects of asphalt oxidation and SBS degradation, with asphalt oxidation being the controlling mechanism. The large temperature fluctuations in the CPA environment suppress the rate of oxidative polymerization, resulting in a delayed heavy-component enrichment process and relatively lower molecular weights compared to single UVA aging.

**Tab 4. Molecular weight data of SBSMA under the two aging modes**

| Index | $M_n$ (g/mol) | $M_w$ (g/mol) | *PDI* | $M_n$ (g/mol) | $M_w$ (g/mol) | *PDI* |
|---|---|---|---|---|---|---|
| SBS-OG | 1180 | 3350 | 2.839 | 1180 | 3350 | 2.839 |
| SBS-R | 1215 | 3560 | 2.930 | 1215 | 3560 | 2.930 |
| Conditions | | UVA | | | CPA | |
| 7D | 1217 | 3554 | 2.920 | 1216 | 3536 | 2.908 |
| 20D | 1218 | 3575 | 2.935 | 1215 | 3528 | 2.904 |
| 60D | 1221 | 3635 | 2.977 | 1218 | 3581 | 2.940 |
| 120D | 1225 | 3745 | 3.057 | 1221 | 3656 | 2.994 |
| 180D | 1229 | 3898 | 3.172 | 1224 | 3754 | 3.067 |

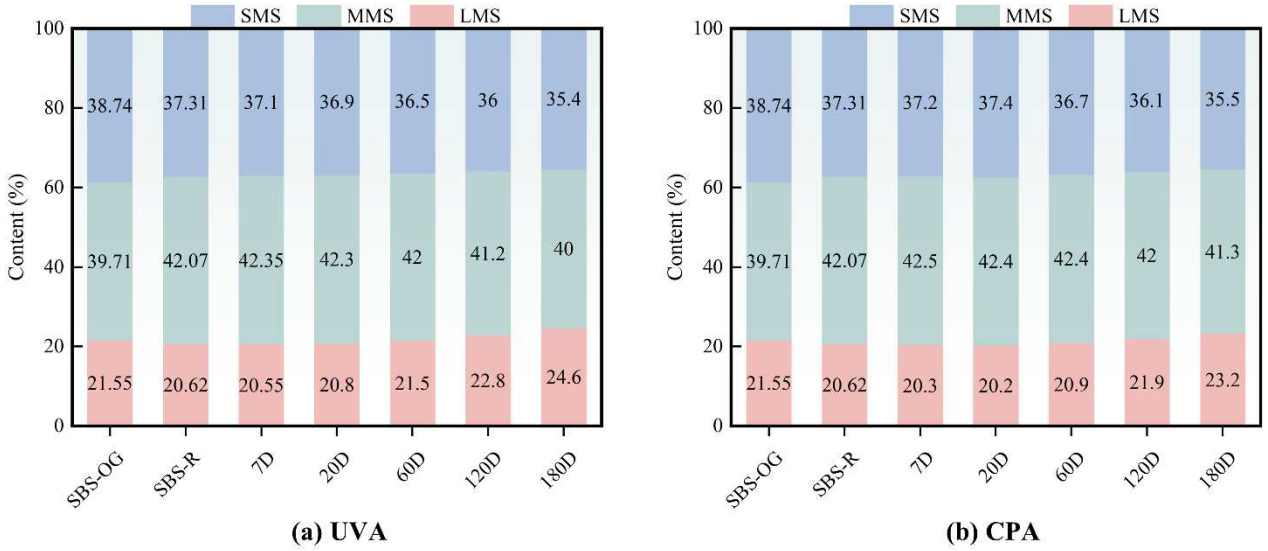


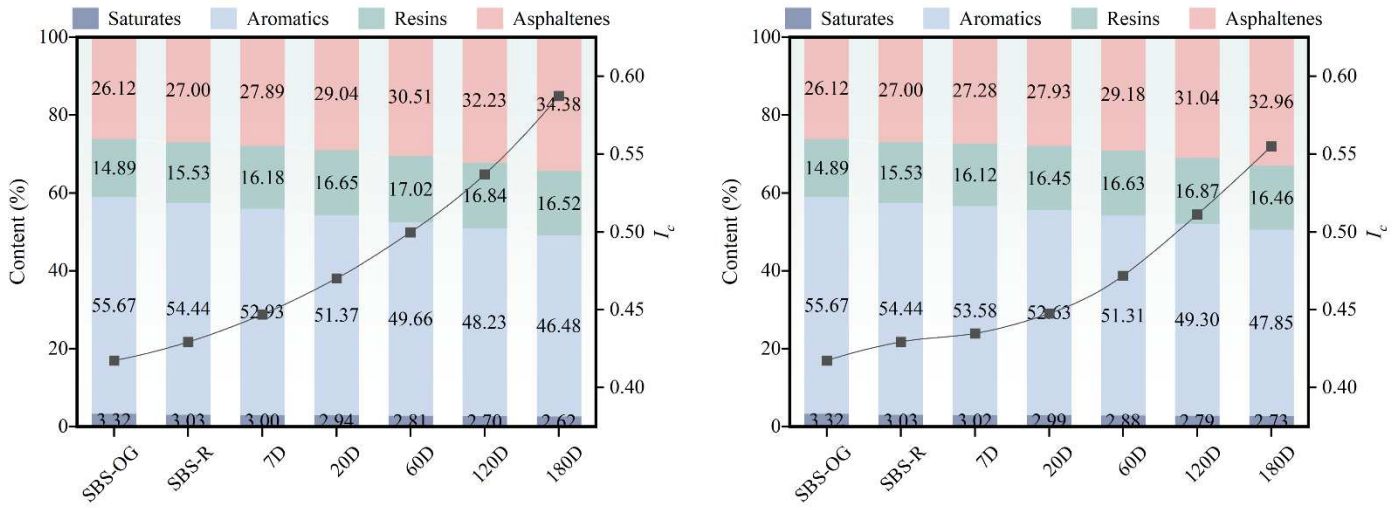

**Fig 17. Molecular weight distribution of SBSMA under the two aging modes**

### 3.3.3 TLC-FID analysis

The SARA four-component distribution and the $I_C$ of the SBSMA specimens under UVA and CPA aging are shown in Fig.18. As aging progresses, the saturate content remains relatively stable with a slight decrease under both aging modes, whereas the aromatic content declines continuously. The resin content first increases and then decreases, while the asphaltene content increases continuously and markedly, leading to a monotonic rise in the $I_C$. After 180 days of aging, the aromatic content of the UVA-180D and CPA-180D specimens decreases by 9.19% and 7.82%, respectively, relative to the unaged SBSMA. Meanwhile, the asphaltene content increases by 8.26% and 6.84%, respectively, compared with the unaged binder. These results indicate that the aging of SBSMA is mainly driven by the conversion of light components into heavy components, in which aromatics and other light fractions are continuously transformed into more polar, higher-molecular-weight asphaltenes through oxidation. The continuous increase in $I_C$ under both aging modes suggests a transition of the SBSMA colloidal structure from a sol type to a gel type, reflecting the overall hardening and embrittlement of the binder.

The different kinetic trajectories of UVA and CPA reveal a staged aging response. In the initial phase, CPA shows a lower oxidation rate than UVA, with less asphaltene accumulation and a smaller $I_C$ increment. This delay in CPA has two causes: the low-temperature phases slow the oxidation kinetics, and the rapid degradation of the SBS polymer provides an additional source of light-molecular fractions. As aging continues, the SBS network is largely depleted, and oxidative

condensation becomes the governing factor in component transformation. At this stage, the UVA-aged samples show a faster oxidation rate. Notably, the $I_C$ acceleration point of CPA at day 60 precedes that of UVA at day 120, consistent with their respective rates of SBS network degradation. Ultimately, by day 180, the $I_C$ values are 40.8% higher for UVA and 33.0% higher for CPA than for the control, confirming that UVA exposure alone produces a more severe oxidative aging state than the coupled plateau conditions. These SARA results provide a chemical basis for the observed macroscopic performance degradation and further support the proposed two-stage aging mechanism of SBSMA.




**(a) UVA** **(b) CPA**

**Fig 18. SARA fractions of SBSMA under the two aging modes**

## 3.4 QTP aging mechanism analysis based on statistical analysis

Based on the preceding morphological, rheological, and compositional findings, a two-stage aging mechanism was identified for SBSMA under UVA and CPA. To verify this mechanism, eight microscopic indicators, namely $R_a$, $R_q$, $I_{SBS}$, $I_{C=O}$, $I_{S=O}$, $I_{PB}$, $PDI$, and $I_C$, were selected for R-type HCA, and representative indicators were subsequently correlated with rheological properties using SRCA.. Finally, four critical aging stages, namely CPA-60D, CPA-180D, UVA-120D, and UVA-180D, were then compared to distinguish the aging pathways under the two protocols. Because only five aging intervals were available, these statistical results were interpreted as trend-level evidence supporting the proposed mechanisms rather than as a predictive model.

### 3.4.1 HCA of microscopic mechanism indicators

Pearson correlation was used to construct a correlation distance matrix for grouping microscopic indicators according to the similarity of their aging trajectories[50,51]. The correlation coefficients of indicators are presented in Fig.19 a and b. Ward's hierarchical clustering involved seven merging steps under each aging condition. The pronounced increase in merging distance between the sixth and seventh steps supported division of the indicators into two clusters, as shown in Fig.19 c and d.

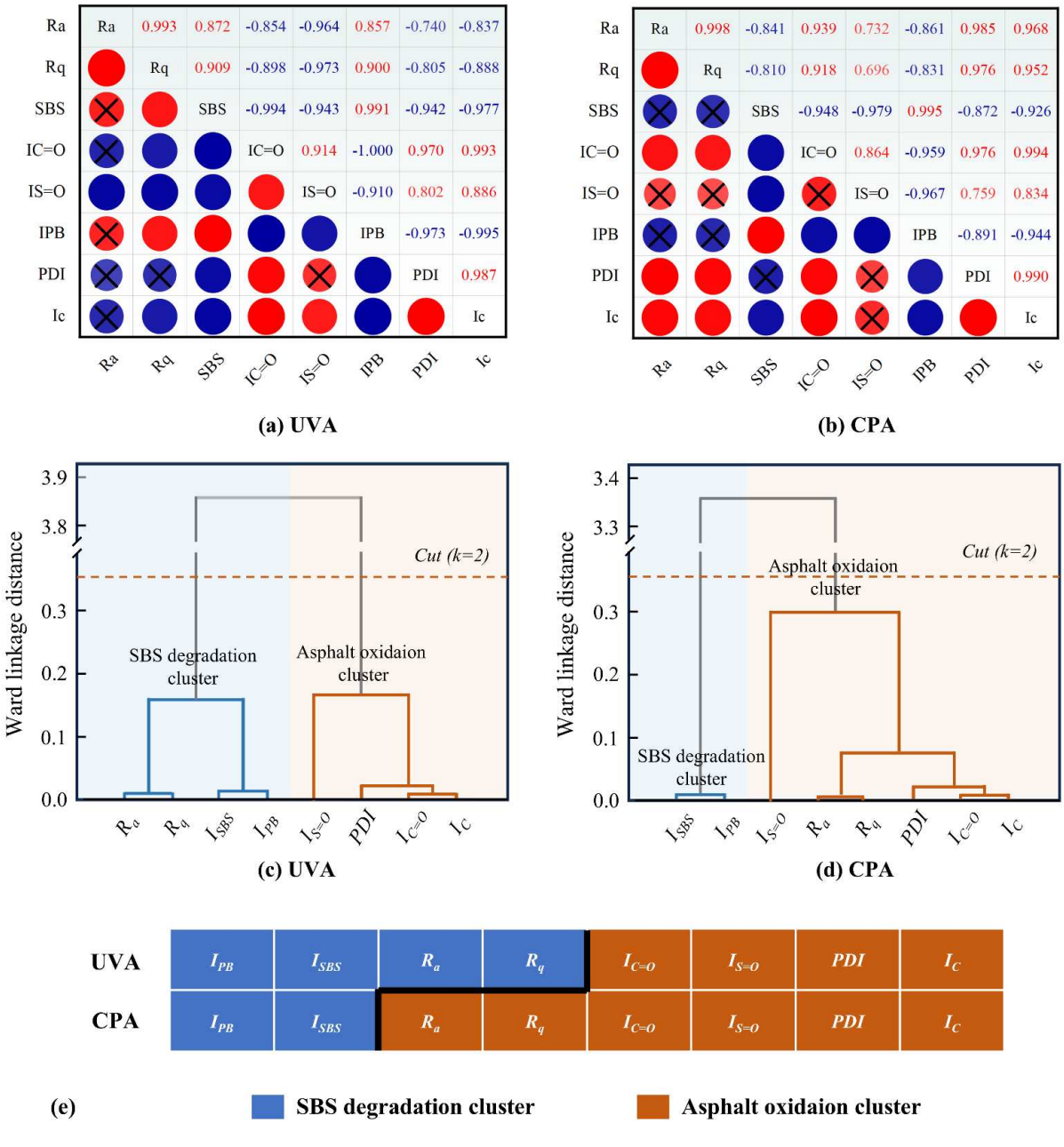



**Fig 19. Correlation analysis among the eight mechanism indicators under the two aging conditions**

The HCA results substantiate the two-stage aging mechanism of SBSMA hypothesized above. $I_{PB}$ and $I_{SBS}$ were grouped into one cluster, with correlation coefficients of 0.995 and 0.991 under CPA and UVA, respectively, both directly characterizing the integrity of the SBS network. By contrast,

778 $I_{C=O}$, $I_{S=O}$, *PDI*, and $I_C$ formed another cluster, in which the correlation coefficient between $I_{C=O}$ and $I_C$
779 exceeded 0.99, collectively reflecting the degree of asphalt oxidation. The correlation distance
780 between the cross-cluster representative indicators $I_{PB}$ and $I_{C=O}$ reached 2.000 under UVA and 1.959
781 under CPA, indicating an almost perfect negative correlation between them. This demonstrates that
782 the two mechanism clusters evolved in opposite directions during aging and could be clearly
783 distinguished. Accordingly, the eight indicators were classified into an SBS degradation cluster and
784 an asphalt oxidation cluster, with $I_{PB}$ and $I_{C=O}$ selected as the representative indicators of each,
785 respectively.

786 Notably, the HCA assignment of $R_a$ and $R_q$ varied with the aging condition. Under UVA, they
787 were incorporated into the SBS degradation cluster, whereas under CPA, they shifted to the asphalt
788 oxidation cluster. This transition corresponds to the reversal of the surface roughness evolution trend
789 under the two aging protocols. Under UVA, the SBSMA surface tended to become smooth owing to
790 the continuous fusion of asphaltenes, leading to a monotonic decrease in $R_a$ and $R_q$ that was consistent
791 with the declining $I_{SBS}$ and $I_{PB}$, so these two indicators were grouped into the SBS degradation cluster.
792 Under CPA, by contrast, $R_a$ and $R_q$ first decreased and then increased. The initial decrease in
793 roughness was attributed to asphaltene aggregation, whereas the subsequent increase was driven by
794 the initiation and propagation of surface micro-cracks under persistent thermal stress, which rendered
795 the surface irregular. At this stage, $R_a$ and $R_q$ evolved in the same direction as the increasing oxidation
796 indicators, and were therefore classified into the asphalt oxidation cluster. This phenomenon indicates
797 that the shift in the cluster membership of $R_a$ and $R_q$ originated from the difference in the surface
798 aging mechanism between the two conditions, further corroborating that thermal-stress-induced
799 micro-cracking is a damage mechanism unique to CPA relative to UVA.

800 3.4.2 SRCA between mechanical indicators and rheological properties

801 Spearman rank correlation evaluates monotonic associations without requiring normality or
802 linearity, making it suitable for comparing microscopic mechanism indicators with rheological
803 properties measured on different scales[52,53]. $I_{PB}$ was selected to represent SBS degradation because
804 it directly reflects the loss of C=C bonds in the PB segment, $I_{C=O}$ was chosen as a direct and widely
805 accepted marker of asphalt oxidation, while $R_a$ was included because its cluster assignment varied

between the two aging conditions. Their correlations with $G^*$, $\delta$, $J_{nr}$, $R$, $N_f$, $S$, and $m$ under UVA and CPA are shown in Fig.20.

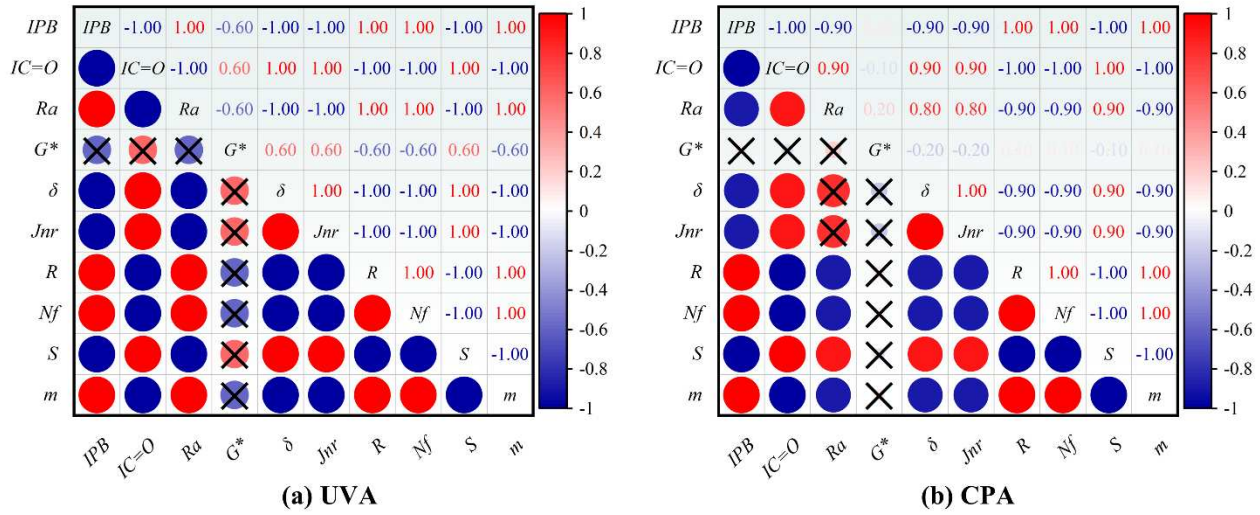



**Fig 20. Spearman rank correlation between mechanism indicators and rheological properties under the two aging conditions**

Fig. 20 reveals that, for both aging protocols, $I_{PB}$ is perfectly positively correlated with $N_f$, $R$, and $m$, and perfectly negatively correlated with $S$. The correlations between $I_{C=O}$ and these rheological parameters are reversed, demonstrating a competitive relationship between SBS degradation and asphalt oxidation in governing the aging performance. The absolute values of the correlation coefficient $\rho$ between $G^*$ and both $I_{PB}$ and $I_{C=O}$ do not exceed 0.600, indicating only a weak correlation with the evolution of $G^*$. This can be attributed to the competing effects of SBS degradation and asphalt oxidation, with the former reducing $G^*$ and the latter increasing it. These opposing effects offset each other during the aging process, resulting in a non-monotonic evolution of $G^*$. This mechanism is the fundamental reason why the $G^*$ evolution of SBSMA differs from that of neat asphalt. Furthermore, the correlations of $\delta$ and $J_{nr}$ with $I_{PB}$ are higher under UVA than under CPA. This is because the oxidation-dominated stage occurs earlier and is more pronounced under CPA, causing $\delta$ and $J_{nr}$ to decline in the late aging stage owing to oxidative hardening, which weakens their correlation with the monotonically decreasing $I_{PB}$. Finally, the relationships between $R_a$ and the rheological properties differ between the two modes. Under UVA, $R_a$ is positively correlated with $N_f$ and $R$ and negatively correlated with $S$, whereas under CPA, $R_a$ is positively correlated with $S$ and negatively correlated with $N_f$. This complexity underscores not only the resolution difference between

the microscopic morphology and the macroscopic performance indicators but also the distinct aging pathways governed by UVA and CPA.

### 3.4.3 Mechanistic insights into critical aging stages

Based on the combined HCA and SRCA, UVA-120D, UVA-180D, CPA-60D, and CPA-180D, four critical aging nodes, were selected to reveal the underlying aging mechanisms. Under UVA, the mechanism shifts at approximately day 120. In the early stage, the rapid decline in $I_{PB}$ indicates that SBS degradation governs the reduction in $N_f$ and $R$, while asphaltene aggregation smooths the surface. Thereafter, the rapid accumulation of $I_{C=O}$ indicates that asphalt oxidation becomes the dominant, increasing $G^*$ and $S$. Under CPA, this transition occurs earlier, at approximately day60. In the early stage, the combined action of UV radiation and temperature fluctuations intensifies the scission of the SBS network, producing a faster decrease in $I_{PB}$ than under UVA. Meanwhile, repeated thermal stress promotes surface microcrack propagation, reversing the initial decrease in $R_a$ caused by asphaltene aggregation. After day 60, SBS degradation gradually slows, and asphalt matrix oxidation increasingly governs the aging response. Nevertheless, the overall oxidation degree under CPA remains lower than that under UVA after long-term aging.

In summary, although both protocols involve competition between SBS degradation and asphalt oxidation, their kinetics and relative contributions differ. Asphalt matrix oxidation is a thermally activated process governed by Arrhenius-type kinetics; therefore, the −20°C stages reduce molecular mobility and the accumulated oxidation rate under CPA[54]. By contrast, the unsaturated PB segments remain susceptible to UV-initiated radical oxidation under the same cumulative UV exposure, while temperature cycling additionally promotes phase separation, interfacial damage, and microcrack propagation[55,56]. Consequently, CPA causes more extensive deterioration of the SBS network and accelerates the transition from SBS degradation to asphalt oxidation, despite producing a lower overall degree of matrix oxidation. The combined loss of SBS network integrity and accumulation of physical microdamage also result in more severe deterioration of fatigue resistance and low-temperature relaxation capacity. Therefore, CPA is more detrimental to the structural integrity of SBSMA than UVA alone.

The aging mechanisms of SBSMA under UVA and CPA conditions are illustrated in Fig. 21.

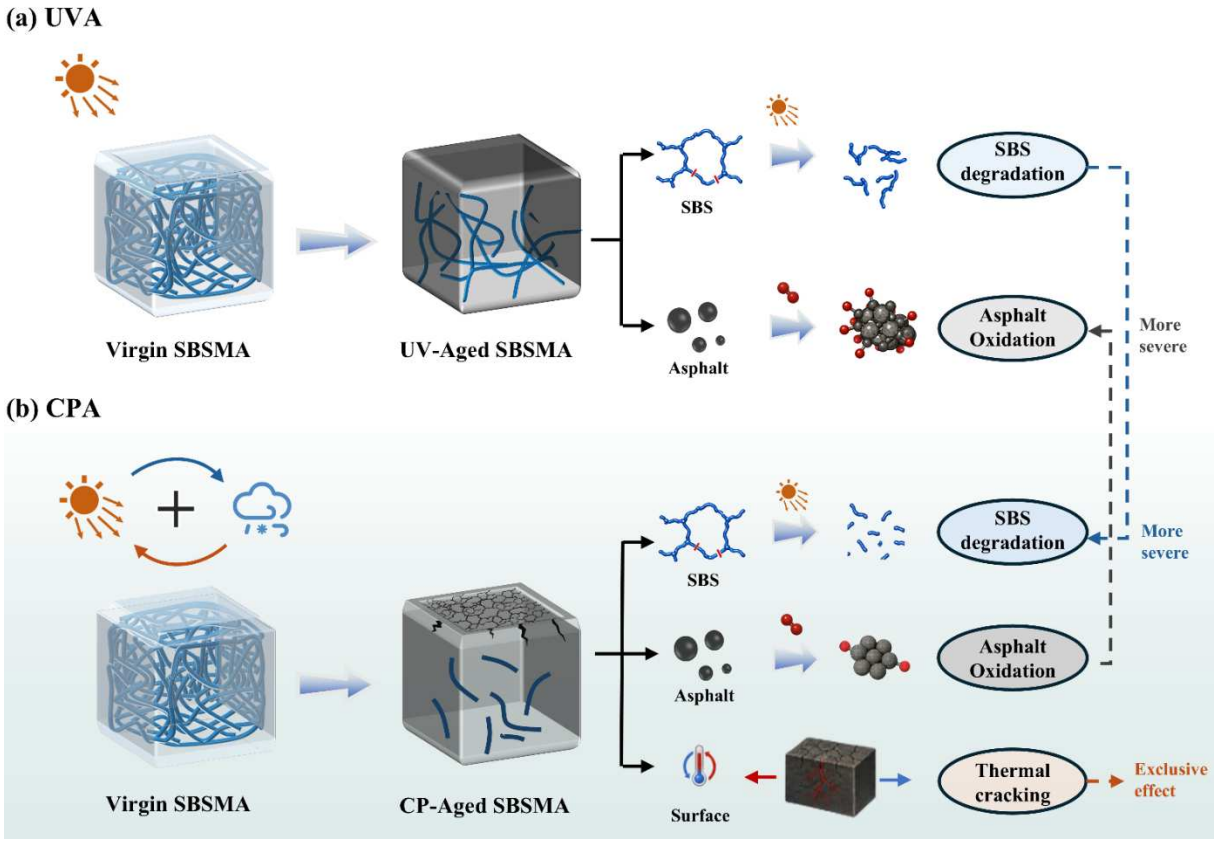



**Fig 21. Schematic diagram of the aging mechanisms under UVA and CPA**

# 4 Conclusions

In this study, a customized aging protocol was developed for SBSMA to simulate the harsh weathering conditions of QTP. By benchmarking the CPA protocol against conventional UVA condition, the behaviours and mechanisms of SBSMA were systematically elucidated through multi-scale morphological, rheological, and chemical characterization, and further corroborated by HCA and SCRA. The main conclusions are as follows:

1) The CPA environment additionally induced surface micro cracks and a more pronounced depletion of the SBS phase. The surface roughness of CPA sample evolved in a non-monotonic manner, indicating a damage mechanism fundamentally different from that associated with UVA.

2) Aging weakened the overall performance of SBSMA, the CPA protocol caused more severe rheological deterioration, with the greatest impact on fatigue resistance and low-temperature cracking.

3) Aging evolution followed a two-stage process, marked by a transition from SBS degradation to oxidative hardening. The CPA protocol accelerated this transition and led to a more rapid depletion of the SBS network, produced a comparatively lower degree of oxidation over the long term, and

caused more severe polymer degradation than UVA.

4) The R-type HCA divided the eight micro-mechanism indices into two clusters, SBS degradation and asphalt oxidation, among which $I_{PB}$ and $I_{SBS}$ were categorized into the SBS degradation cluster, whereas $I_{C=O}$, $I_{S=O}$, *PDI*, and $I_C$ belonged to the asphalt oxidation cluster; the classification of $R_a$ and $R_q$ varied depending on the aging conditions.

There are several limitations of the present study that warrant further investigation:

1) The statistical robustness of the current trend analysis is limited by only five aging intervals. With more comprehensive time series and performance data, future studies could develop robust quantitative models of SBSMA aging under complex environmental conditions.

2) Quantifying the effect of thermally induced stress damage in asphalt binders subjected to large diurnal temperature fluctuations remains a critical and unresolved direction for future work.

3) The thickness of the aged binder specimens introduced a vertical aging gradient, limiting quantitative correlations between surface and bulk binder. Future studies should employ thinner films or layer specific characterizations.

# Declaration of Competing Interest

The authors declare that they have no known competing financial interests or personal relationships that could have appeared to influence the work reported in this paper.

# Acknowledgments

This work was supported by the National Natural Science Foundation of China (**No. 52378464**), Natural Science Foundation of Sichuan (**No. 2024NSFSC0168, No. 2025ZNSFSC0033)**, and Scientific Research and Development Program of China Communications Construction Group Co., Ltd. **(No. 2025-GNBKJ-01).** The authors would like to thank Analytical and Testing Center of Southwest Jiaotong University for SEM, AFM and GPC tests.

# References

[1] A. Sha, B. Ma, H. Wang, L. Hu, X. Mao, X. Zhi, H. Chen, Y. Liu, F. Ma, Z. Liu, R. He, W. Si, X. Wang, C. Li, Highway constructions on the Qinghai-Tibet Plateau: Challenge, research and practice, J. Road Eng. 2 (2022) 1–60.

https://doi.org/10.1016/j.jreng.2022.02.002.

[2] L. Zhang, H. Wang, C. Xing, Y. Tan, Deterioration of low-temperature property of modified asphalt under ultraviolet ageing considering physical hardening, Road Mater. Pavement Des. 27 (2026) 152–177. https://doi.org/10.1080/14680629.2025.2482847.

[3] B. Li, M. Liu, Y. Mu, J. Luo, X. Ju, F. Yin, F. Yu, Y. Huang, Distribution and evolution of distress in embankment-bridge transition sections of the Gonghe–Yushu Expressway in degrading permafrost regions, Transp. Geotech. 58 (2026) 101945. https://doi.org/10.1016/j.trgeo.2026.101945.

[4] Z. Zhang, Q. Wu, Y. Liu, Z. Zhang, G. Wu, Thermal accumulation mechanism of asphalt pavement in permafrost regions of the Qinghai–Tibet Plateau, Appl. Therm. Eng. 129 (2018) 345–353. https://doi.org/10.1016/j.applthermaleng.2017.10.065.

[5] Y. Xie, J. Zheng, Y. Luo, G. Chen, X. Li, D. Ren, Analysis of temperature field variation characteristics and influencing factors of asphalt pavement under large temperature variation, J. Therm. Anal. Calorim. (2026). https://doi.org/10.1007/s10973-026-15520-5.

[6] Q. Ma, T. Lan, Y. Lai, X. Luo, P. He, Application of the cooling measures in the highway roadbed in permafrost regions of the Qinghai-Tibet Plateau, Cold Reg. Sci. Technol. 221 (2024) 104177. https://doi.org/10.1016/j.coldregions.2024.104177.

[7] M. Chai, Y. Mu, J. Zhang, W. Ma, G. Liu, J. Chen, Characteristics of Asphalt Pavement Damage in Degrading Permafrost Regions: Case Study of the Qinghai–Tibet Highway, China, J. Cold Reg. Eng. 32 (2018) 05018003. https://doi.org/10.1061/(ASCE)CR.1943-5495.0000165.

[8] S. Zhou, J. Yan, B. Shi, S. Li, C. Ai, C. Yan, Green synthesis of a broad-spectrum UV-blocking bitumen modifier: Investigation of anti-aging performance and mechanism in bitumen, J. Clean. Prod. 425 (2023) 139064. https://doi.org/10.1016/j.jclepro.2023.139064.

[9] D. Adwani, J. Mirwald, G. Pipintakos, A. Sreeram, R. Hajj, A. Bhasin, Historical insights on asphalt aging, mechanisms, and anti-aging technologies with evaluation of a potential antioxidant as the way forward, Constr. Build. Mater. 493 (2025) 143055. https://doi.org/10.1016/j.conbuildmat.2025.143055.

[10] L. Kong, S. Su, Z. Wang, P. Wu, Y. Zhang, Z. Chen, D. Ren, C. Ai, Microscale mechanism and key factors of waterborne epoxy resin emulsified asphalt enhancing interlayer bonding performance and shear resistance of bridge deck pavement, Constr. Build. Mater. 419 (2024) 135570. https://doi.org/10.1016/j.conbuildmat.2024.135570.

[11] R. Polo-Mendoza, G. Martinez-Arguelles, L.F. Walubita, F. Moreno-Navarro, F. Giustozzi, L. Fuentes, T.

926 Navarro-Donado, Ultraviolet ageing of bituminous materials: A comprehensive literature review from 2011 to 2022,
927 Constr. Build. Mater. (2022).
928 [12] E.A. O'Rear, L. Huang, M. Zaman, Evolution of Model Compounds and Functional Group Compositions for
929 Molecular Dynamics Simulations of Aged Asphalt Binder, Molecules 30 (2025) 4476.
930 https://doi.org/10.3390/molecules30224476.
931 [13] M. Ahmad, M. Khedmati, D. Mensching, B. Hofko, H. F. Haghshenas, Aging characterization of asphalt binders
932 through multi-aspect analyses: A critical review, Fuel 376 (2024) 132679.
933 https://doi.org/10.1016/j.fuel.2024.132679.
934 [14] R. Hossain, N.M. Wasiuddin, Evaluation of Degradation of SBS Modified Asphalt Binder Because of RTFO,
935 PAV, and UV Aging using a Novel Extensional Deformation Test, Transp. Res. Rec. J. Transp. Res. Board 2673
936 (2019) 447–457. https://doi.org/10.1177/0361198119847471.
937 [15] K. Liu, Y. Xu, Z. Xing, Y. Li, Z. Sun, H. Wang, Effects of natural weathering in cold regions on the
938 morphological structure, rheological properties, and molecular characteristics of asphalt binders, Constr. Build.
939 Mater. 493 (2025) 143172. https://doi.org/10.1016/j.conbuildmat.2025.143172.
940 [16] M. Liang, M. Guo, L. Wang, C. Li, Y. Tan, A study on multi-scale evaluation methods of field aging of bitumen
941 in cold and arid regions, Constr. Build. Mater. 497 (2025) 143908.
942 https://doi.org/10.1016/j.conbuildmat.2025.143908.
943 [17] Z. Ju, D. Ge, S. Lv, Q. Liu, X. Wang, Y. Bai, Rheological and microscopic characterization and correlation
944 analysis of asphalt under high-intensity ultraviolet radiation, Case Stud. Constr. Mater. 21 (2024) e03552.
945 https://doi.org/10.1016/j.cscm.2024.e03552.
946 [18] Z. He, J. Geng, W. Zhao, J. Liu, C. Qi, R. Qi, L. Huang, Road performance and chemical evolution of aged
947 asphalt subjected to intense ultraviolet radiation and large temperature fluctuations, Fuel 394 (2025) 135104.
948 https://doi.org/10.1016/j.fuel.2025.135104.
949 [19] X. Ma, S. Song, S. Qiu, Climatic influences on vertical asphalt aging: A two-year field study and molecular-
950 level analysis, Case Stud. Constr. Mater. 23 (2025) e05607. https://doi.org/10.1016/j.cscm.2025.e05607.
951 [20] Y. Zhao, X. Wu, Y. Chao, N. Liang, P. Zhou, Z. Li, Y. Mei, Aging characteristics and microscopic mechanisms
952 of SBS asphalt based on coupled light–heat–water aging, Constr. Build. Mater. 456 (2024) 139190.
953 https://doi.org/10.1016/j.conbuildmat.2024.139190.
954 [21] T. Fan, S. Han, C. Si, Fatigue performance of calcium sulfate whisker-modified asphalt under multi-modal

aging conditions, J. Clean. Prod. 494 (2025) 144976. https://doi.org/10.1016/j.jclepro.2025.144976.

[22] A. Rajib, S. Saadeh, P. Katawal, B. Mobasher, E.H. Fini, Enhancing Biomass Value Chain by Utilizing Biochar as A Free Radical Scavenger to Delay Ultraviolet Aging of Bituminous Composites Used in Outdoor Construction, Resour. Conserv. Recycl. 168 (2021) 105302. https://doi.org/10.1016/j.resconrec.2020.105302.

[23] J. Hu, S. Wu, Q. Liu, M.I. García Hernández, Z. Wang, S. Nie, G. Zhang, Effect of ultraviolet radiation in different wavebands on bitumen, Constr. Build. Mater. 159 (2018) 479–485. https://doi.org/10.1016/j.conbuildmat.2017.10.117.

[24] R. Wang, J. Yue, R. Li, Y. Sun, Evaluation of aging resistance of asphalt binder modified with graphene oxide and carbon nanotubes, J. Mater. Civ. Eng. 31 (2019) 04019274. https://doi.org/10.1061/(ASCE)MT.1943-5533.0002934.

[25] X. Xie, T. Hui, Y. Luo, H. Li, G. Li, Z. Wang, Research on the properties of low temperature and anti‐UV of asphalt with nano‐ZnO/nano‐$TiO_2$ /copolymer SBS composite modified in high‐altitude areas, Adv. Mater. Sci. Eng. 2020 (2020) 9078731. https://doi.org/10.1155/2020/9078731.

[26] A.M. Hung, M. Kazembeyki, C.G. Hoover, E.H. Fini, Evolution of Morphological and Nanomechanical Properties of Bitumen Thin Films as a Result of Compositional Changes Due to Ultraviolet Radiation, ACS Sustain. Chem. Eng. 7 (2019) 18005–18014. https://doi.org/10.1021/acssuschemeng.9b04846.

[27] S. Zhou, K. Long, S. Zhu, S. Li, C. Ai, C. Yan, Investigation of the Morphological Characteristics and Chemical Properties of Hardened Layers in Polymer-Modified Asphalt during Aging, J. Mater. Civ. Eng. 37 (2025) 04025349. https://doi.org/10.1061/JMCEE7.MTENG-20588.

[28] L. Kong, Z. Wang, S. Su, J. Yue, W. Luo, S. Zhou, D. Ren, C. Ai, Exploring the interplay between thermo-oxidative degradation and asphalt aging in thermoplastic polyurethane-modified asphalt: Mechanisms, properties, and performance evolution, Constr. Build. Mater. 412 (2024) 134694. https://doi.org/10.1016/j.conbuildmat.2023.134694.

[29] S.S. Pandhawale, S. Jain, A.K. Chandrappa, V. Kari, UV aging assessment of asphalt binder: Influence of duration, zinc oxide, and aging condition, Int. J. Pavement Eng. 25 (2024) 2359537. https://doi.org/10.1080/10298436.2024.2359537.

[30] M. Guo, M. Liang, X. Du, Evaluation on Feasibility of Carbon Black and Hindered Amine Light Stabilizer as UV-Resistant Additives of Asphalt Binder, J. Test. Eval. 51 (2023) 3987–4003. https://doi.org/10.1520/JTE20220611.

[31] M. Lin, Y. Fan, L. Zhang, P. Li, R. Ye, Y. Zhang, Fatigue characteristics of recycled asphalt mastic under strong ultraviolet radiation in gansu, China, Case Stud. Constr. Mater. 22 (2025) e04340. https://doi.org/10.1016/j.cscm.2025.e04340.

[32] H. Li, C. Xing, B. Zhu, X. Zhang, Y. Gao, S. Tang, H. Cheng, Comparative analysis of four styrene-butadiene-styrene (SBS) structure repair agents in the rejuvenation of aged SBS-modified bitumen, Constr. Build. Mater. 476 (2025) 141232. https://doi.org/10.1016/j.conbuildmat.2025.141232.

[33] S. Singh, N. Mittal, H. Singh, D. Oliva, Improving the segmentation of digital images by using a modified otsu's between-class variance, Multimed. Tools Appl. 82 (2023) 40701–40743. https://doi.org/10.1007/s11042-023-15129-y.

[34] Y. Xu, K. Niu, H. Zhu, R. Chen, L. Ou, J. Wang, Generation and evolution mechanisms of asphalt aging under the combined effects of intense UV radiation and large temperature variations, Constr. Build. Mater. 438 (2024) 136786. https://doi.org/10.1016/j.conbuildmat.2024.136786.

[35] M. Li, M. Hu, S. Ji, Y. Meng, L. Yuan, Effects of aging on the nanoscale phase characteristics of bitumen: Insights from chemical composition analysis, Fuel 385 (2025) 134160. https://doi.org/10.1016/j.fuel.2024.134160.

[36] S. Zhou, J. Wang, S. Li, C. Yan, Investigating the rheological behaviour of styrene–butadiene–styrene modified asphalt, Road Mater. Pavement Des. 25 (2024) 1964–1979. https://doi.org/10.1080/14680629.2023.2287715.

[37] C. Zhu, Z. Xu, H. Zhang, Z. Wang, D. Li, N. Su, D. Zhang, Rheological and micro characteristics of asphalt containing different nanocomposite ratios of CeO2/MMT during thermal-oxidative and ultraviolet aging, Constr. Build. Mater. 495 (2025) 143732. https://doi.org/10.1016/j.conbuildmat.2025.143732.

[38] H. Chen, H.U. Bahia, Proposed asphalt binder fatigue criteria for various traffic conditions using the LAS or the G-R parameters, Mater. Struct. 55 (2022) 24. https://doi.org/10.1617/s11527-022-01883-2.

[39] T. Xia, X. Chen, J. Xu, A. Zhang, Z. Wang, X. Chen, X. Xia, Y. Li, Key role of network formation in rutting, fatigue and brittle performance of bitumen/PEG/MDI/SiO2 composites, Constr. Build. Mater. 296 (2021) 123739. https://doi.org/10.1016/j.conbuildmat.2021.123739.

[40] S. Zhou, J. Yan, W. Ning, S. Li, C. Ai, C. Yan, Performance and Mechanism of Using Low-Cost Fumed Silica Nanoparticles in Enhancing High Viscosity Modified Asphalt, Constr. Build. Mater. 409 (2023) 134090. https://doi.org/10.1016/j.conbuildmat.2023.134090.

[41] A. Badughaish, A.S. Mohamed, M. Alae, S. Amirkhanian, F. Xiao, Influence mechanism of crumb rubber pretreatment and antioxidants on aging and cracking behavior of rubberized asphalt, Constr. Build. Mater. 514 (2026)

145625. https://doi.org/10.1016/j.conbuildmat.2026.145625.
[42] S. Liu, H. Wang, J. Yang, Assessment and mechanism of antioxidant activity of phenols as asphalt antioxidants, Int. J. Pavement Eng. 25 (2024) 2335316. https://doi.org/10.1080/10298436.2024.2335316.
[43] M. Hu, D. Sun, G. Sun, Y. Sun, J. Ouyang, Performance study on anti-weather aging combinations for high-content polymer modified asphalt and comparison by improved multi-scale mathematical TOPSIS method, Constr. Build. Mater. 407 (2023) 133357. https://doi.org/10.1016/j.conbuildmat.2023.133357.
[44] A. Jada, M. Salou, Effects of the asphaltene and resin contents of the bitumens on the water–bitumen interface properties, J. Pet. Sci. Eng. 33 (2002) 185–193. https://doi.org/10.1016/S0920-4105(01)00185-1.
[45] S. Li, Y. Wang, S. Zhou, Investigation of purified lignin as an antioxidant for sustainable bitumen, Constr. Build. Mater. 458 (2025) 139499. https://doi.org/10.1016/j.conbuildmat.2024.139499.
[46] A. Margaritis, H. Soenen, E. Fransen, G. Pipintakos, G. Jacobs, J. Blom, W. Van Den Bergh, Identification of ageing state clusters of reclaimed asphalt binders using principal component analysis (PCA) and hierarchical cluster analysis (HCA) based on chemo-rheological parameters, Constr. Build. Mater. 244 (2020) 118276. https://doi.org/10.1016/j.conbuildmat.2020.118276.
[47] J. Zhu, S. Yang, D. Shen, F. Zhang, R. Cao, C. Wu, B. Jin, S. Wu, Selection of representative molecules of asphalt aromatics based on principal component analysis and hierarchical clustering, Mol. Simul. 50 (2024) 881–898. https://doi.org/10.1080/08927022.2024.2364702.
[48] H. Ni, M. Hu, D. Sun, L. Xu, S. Ling, T. Lu, Y. Deng, Degradation characteristics of SBS polymer and its contribution to weathering aging of modified asphalt, Constr. Build. Mater. 369 (2023) 130549. https://doi.org/10.1016/j.conbuildmat.2023.130549.
[49] W. Xiong, Y. Liu, Y. Muhammad, F. Han, L. Yang, X. Jin, Z. Zhao, J. Li, MXene by regulating etching conditions enhanced UV resistance of SBS modified asphalt: Evaluating asphalt photo-oxidation and SBS degradation, Constr. Build. Mater. 377 (2023) 131006. https://doi.org/10.1016/j.conbuildmat.2023.131006.
[50] E. Mohammadi Golafshani, A. Behnood, M.M. Karimi, Predicting the dynamic modulus of asphalt mixture using hybridized artificial neural network and grey wolf optimizer, Int. J. Pavement Eng. 24 (2023) 2005056. https://doi.org/10.1080/10298436.2021.2005056.
[51] X. Zhang, B. Tang, X. Cao, J. Li, H. Zhu, Study on the release characteristics of volatile organic compounds from different aged asphalt, J. Clean. Prod. 423 (2023) 138774. https://doi.org/10.1016/j.jclepro.2023.138774.
[52] R. Zhang, T. Cheng, Y. Lu, H. Luo, J. Huang, Evaluating and correlating asphalt binder and mixture fatigue

1042 properties considering aging conditions, Constr. Build. Mater. 436 (2024) 136356.
1043 https://doi.org/10.1016/j.conbuildmat.2024.136356.
1044 [53] Y. Wen, Q. Liu, L. Chen, J. Pei, J. Zhang, R. Li, Review and comparison of methods to assess the storage
1045 stability of terminal blend rubberized asphalt binders, Constr. Build. Mater. 258 (2020) 119586.
1046 https://doi.org/10.1016/j.conbuildmat.2020.119586.
1047 [54] R.R. Glaser, J.F. Schabron, T.F. Turner, J.-P. Planche, S.L. Salmans, J.L. Loveridge, Low-temperature oxidation
1048 kinetics of asphalt binders, Transp. Res. Rec. J. Transp. Res. Board 2370 (2013) 63–68.
1049 https://doi.org/10.3141/2370-08.
1050 [55] V. Mouillet, F. Farcas, S. Besson, Ageing by UV radiation of an elastomer modified bitumen, Fuel 87 (2008)
1051 2408–2419. https://doi.org/10.1016/j.fuel.2008.02.008.
1052 [56] H. Xu, H. Zhan, M. Wang, Y. Tan, Microstructural characteristics evolution of asphalt mastics under cyclic
1053 environmental temperature variations, Constr. Build. Mater. 400 (2023) 132795.
1054 https://doi.org/10.1016/j.conbuildmat.2023.132795.
1055